

11. SITE 783¹

Shipboard Scientific Party²

HOLE 783A

Date occupied: 24 March 1989
Date departed: 26 March 1989
Time on hole: 1 day, 5 hr, 45 min
Position: 30°57.86'N, 141°47.27'E
Bottom felt (rig floor; m; drill-pipe measurement): 4660.0
Distance between rig floor and sea level (m): 11.20
Water depth (drill-pipe measurement from sea level; m): 4648.8
Total depth (rig floor; m): 4828.20
Penetration (m): 168.20
Number of cores: 18
Total length of cored section (m): 168.20
Total core recovered (m): 46.95
Core recovery (%): 27.9

Oldest sediment cored:

Depth (mbsf): 150.27
Nature: glass-rich silty clay, sheared phacoidal serpentine
Earliest age: early Pliocene(?)
Measured velocity (km/s): 1.6

Hard rock:

Depth (mbsf): 158.60
Nature: serpentinitized ultramafic rock

Principal results: Site 783 is located on the northern, midflank part of a seamount that forms part of a 500-km-long ridge running along the lowermost, inner wall of the Izu-Bonin Trench. The single hole, 783A, attempted at this site was drilled to 168.2 m below seafloor (mbsf) with 27.9% recovery before being abandoned because of high torque. Two lithologic units were defined. Unit I, from 0 to 120.0 mbsf, is middle or lower Pleistocene to lower Pliocene or older, glass-rich, silty clay to claystone. Unit II (120.0–158.6 mbsf) is phacoidal sheared serpentine with clasts of serpentinitized harzburgite and metabasalt. The harzburgite has a primary mineralogy of olivine (80–90 modal%) and orthopyroxene (10–15 modal%) with minor clinopyroxene and spinel. Thus, the seamount is confirmed as serpentinite in composition, although the early Pliocene or older age demonstrates that it predates the Mariana serpentinite seamount drilled at Sites 778 through 780.

Shear fabrics and convolute plastic folding indicative of post-emplacement tectonic activity can be seen within the claystones of Unit I and the phacoidal serpentine of Unit II. Studies of physical properties show that the bulk densities increase from 1.47 to 1.59 g/cm³ in the sediments of Unit I and cluster at about 2.1 g/cm³ in the serpentine of Unit II. The average compressional-wave velocity in the sediments is 1.9 km/s. Thermal conductivities average about 1 W/mK in sediments and 1.91 W/mK in the serpentine. Heat flow in the sediments is 23 mW/m². Interstitial fluids show a sharp chemical discontinuity at the sediment/serpentine boundary with rapid chemical changes thereafter, which include increases in

pH, calcium, and sodium, depletions in silica, magnesium, sulfate, and potassium, and little change in chlorinity. The fluid chemistry, therefore, shows that serpentinitization is still taking place, but without the low-chlorinity component identified at the Mariana seamount (Sites 778 through 780).

BACKGROUND AND SCIENTIFIC OBJECTIVES

The eastern 50 km of the Izu-Bonin forearc is morphologically, compositionally, and structurally different from the remainder of the forearc. Within 50 km of the trench axis, a ridge runs for more than 500 km along the lowermost, inner wall of the Izu-Bonin Trench, at a latitude of about 30°N (Fig. 1). This ridge is separated from the outer-arc high by a narrow (~10 km wide) sediment trough, which has a series of seamounts along its eastern and western boundaries. Dredges from two of these seamounts, one at 32°N (K. Saboda, pers. comm., 1987) and the other at about 31°N (Kobayashi, 1989), recovered serpentinitized ultramafic rocks. The seamount at 31°N, chosen for Ocean Drilling Program (ODP) Site 783, was dredged in 1988 at three locations (Fig. 2), yielding a wide variety of sedimentary, igneous, and metamorphic rocks (Kobayashi, 1989). Most of the samples dredged from the two summit locations are serpentinitized ultramafic and mafic rocks, showing slickensides and fractures. Some pumice fragments and sedimentary rocks were also retrieved from the summit and these comprise the bulk of the rocks recovered from the lower west flank of the seamount. A very small amount of serpentine mud adhering to the surfaces of a few of the metamorphosed rocks was recovered.

Several multichannel seismic lines were run across the inner trench wall region, and the structure of the ridge and the seamounts within it are presented in Horine et al. (this volume). The presence of fault planes associated with the seamounts and detected within the ridge suggests that the ridge is still tectonically active. By comparison with Conical Seamount, the seamount at Site 783 is far more complex. The summit region of this seamount is broken by numerous small fault blocks and lacks coherent reflectors ("Underway Geophysics" chapter, this volume). Thus, the seamount is most likely not currently producing serpentine flows, but may be, however, a formerly active serpentinite diapir. The study of the interstitial waters within the sediments (both pelagic and serpentine) at this site is critical to the understanding of the history of this seamount, the flux of subduction-derived fluids through the outer forearc wedge, and the interaction of serpentinite with the associated country rock and overlying sediments.

The history of sedimentation in this part of the forearc has not been studied in detail. The rate of recent sedimentation in this part of the forearc, though expected to be lower than the rate closer to the active arc, is constrained only by seismic profiling. The sequence, if condensed, should provide a comprehensive history of outer-forearc sedimentation as well as a record of the interaction between pelagic sedimentation and influx from seamount serpentinite. In addition, an influx of arc-derived sediment is likely from cross-arc transport via the

¹ Fryer, P., Pearce, J. A., Stokking, L. B., et al., 1990. *Proc. ODP, Init. Repts.*, 125: College Station, TX (Ocean Drilling Program).

² Shipboard Scientific Party is as given in the list of participants preceding the contents.

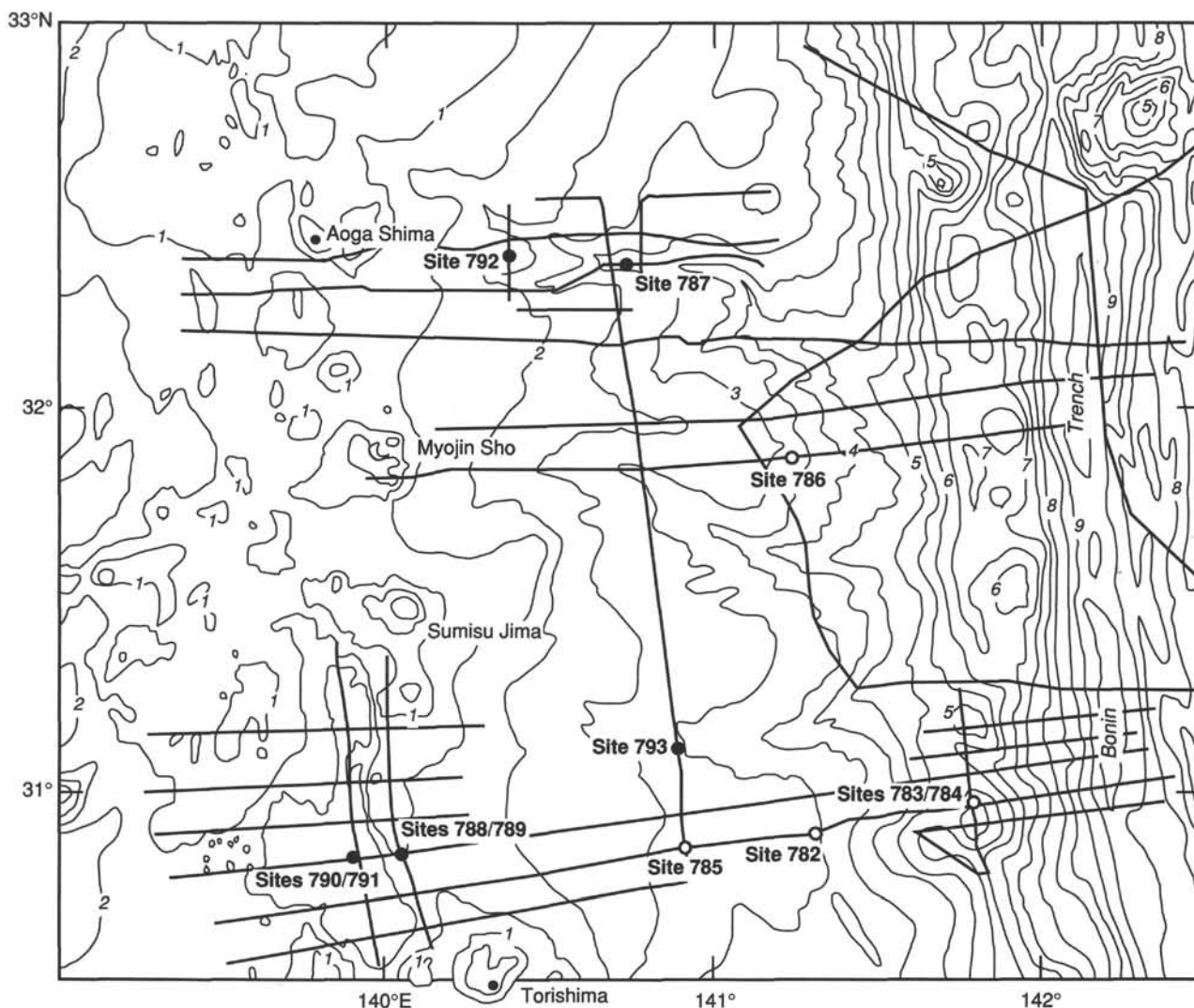


Figure 1. Location of sites in the Izu-Bonin forearc from Legs 125 and 126. Note the north-trending ridge on the inner trench wall. Site 783 was located at proposed Site BON-7. Crosses represent dredge sites on two seamounts of the outer forearc ridge, one at 32°N and the other at Site 783 at 31°N. Bathymetry in kilometers.

large canyon systems of the Izu-Bonin forearc. North of the seamount, a reentrant in the outer forearc ridge forms part of the distal portion of a prominent canyon system that stretches more than halfway across the forearc. Some of the sediment filling this part of the canyon laps onto the seamount. Thus, the nature of sediment transport along this channel can be investigated by drilling into the material on the north flank of the seamount.

The objectives of drilling at this site were as follows: (1) to determine the nature of sediments in the outermost forearc region; (2) to study the sedimentary sequences on the flank of the seamount, and hence to constrain the regional tectonic history of the ridge upon which the seamount is located, the age of the seamount, and the mode of emplacement of the seamount; (3) to study the composition and structure of basement underlying the sedimentary column in order to determine whether the seamount is a block of upfaulted lower crustal material or an older, tectonized analog of Conical Seamount; and (4) to determine the composition of interstitial waters present in the sediments. To achieve these objectives, Site 783 was located at 30°57.86'N, 140°47.27'E, in a water depth of 4648.8 m, on the northern, midflank part of the

seamount (Fig. 1). The sediment cover over acoustic basement is approximately 200 m (see "Underway Geophysics" chapter, this volume).

OPERATIONS

Transit from Sites 782 to 783 (Proposed Site BON-7)

After a 26-nmi transit from Site 782, Site 783 was established at 2030UTC, 23 March 1989, by the deployment of a beacon.

Hole 783A

Because the nature of the material on the surface at Site 783 was unclear from the seismic records, a standard rotary core barrel (RCB) bottom-hole assembly with a hydraulic bit release was deployed. The pipe trip began at 2200UTC, 23 March, and Hole 783A was spudded at 0500UTC, 24 March. The first RCB retrieval recovered 9.71 m of core, establishing the mud line at 4648.8 m below sea level (mbsl). Recovery was sporadic in the lithologic units rich in ash, silt, and serpentine. No notable problems occurred until Core 125-783A-18R was being cut, when drill-string torque and circulation pressure

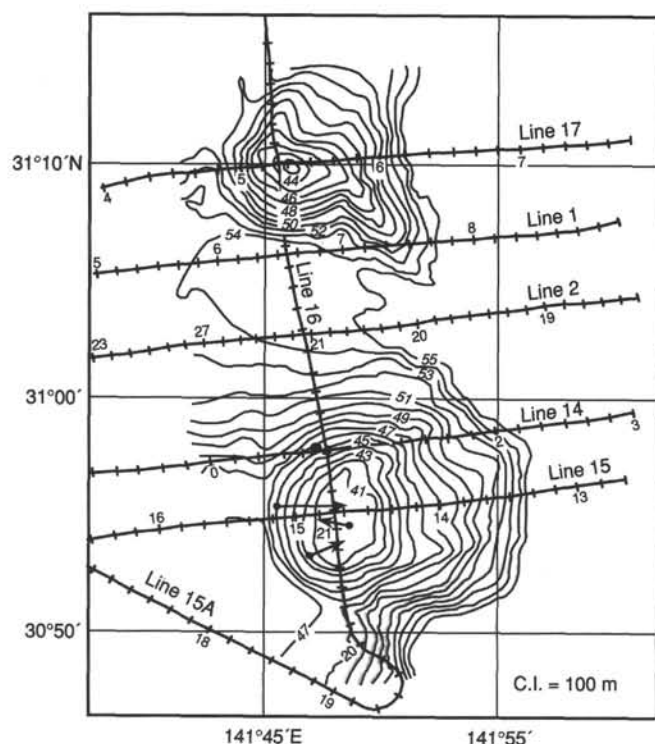


Figure 2. Bathymetry of the inner trench wall seamounts at 31°N. Site 783 is located on the north flank of the southern seamount. Arrows mark the tracks of three dredge hauls made on the seamount in 1988 (Kobayashi, 1989).

increased considerably. A mud pill, circulation of high-viscosity mud, and a wiper trip did not improve hole conditions, so the hole was abandoned.

The RCB was deployed 18 times to a total depth of 168.2 mbsf in Hole 783A, recovering 46.95 m of core for a recovery rate of 27.9% (Table 1). Heat-flow measurements were taken at 42.7 and 90.0 mbsf. Site 783 officially ended at 0215UTC, 26 March, when the drill string was pulled to 4088.8 mbsl and the vessel was under way for Site 784 in dynamic positioning mode.

Table 1. Coring summary for Site 783.

Core no.	Date (March 1989)	Time (UTC)	Depth (mbsf)	Length cored (m)	Length recovered (m)	Recovery (%)
125-783A-						
1R	24	0630	0.0-9.7	9.7	9.71	100.0
2R	24	0800	9.7-16.4	6.7	1.89	28.2
3R	24	0920	16.4-26.0	9.6	0.02	0.2
4R	24	1050	26.0-35.7	9.7	6.72	69.3
5R	24	1210	35.7-42.7	7.0	5.25	75.0
6R	24	1500	42.7-52.4	9.7	0.00	0.0
7R	24	1610	52.4-62.1	9.7	4.70	48.4
8R	24	1720	62.1-71.8	9.7	4.33	44.6
9R	24	1815	71.8-81.3	9.5	0.02	0.2
10R	24	1915	81.3-90.9	9.6	1.87	19.5
11R	24	2230	90.9-100.6	9.7	0.22	2.3
12R	25	0000	100.6-110.2	9.6	0.40	4.2
13R	25	0230	110.2-119.9	9.7	0.11	1.1
14R	25	0500	119.9-129.6	9.7	0.42	4.3
15R	25	0800	129.6-139.2	9.6	4.49	46.8
16R	25	1140	139.2-148.9	9.7	3.87	39.9
17R	25	1500	148.9-158.6	9.7	1.67	17.2
18R	25	1750	158.6-168.2	9.6	1.26	13.1
Coring totals				168.2	46.95	27.9

LITHOSTRATIGRAPHY

The stratigraphic section recovered at Site 783 is divided into two lithologic units: lithologic Unit I, composed primarily of olive brown (2.5Y 4/4) to greenish-gray (5G 4/1) vitric clayey silt and glass-rich silty clay or claystone, and lithologic Unit II, composed of greenish-gray (5GY 6/1 to 5GY 4/1) and bluish-gray (5B 6/1 to 5B 4/1) phacoidal, sheared serpentine with vertical convolute bedding (Table 2).

Lithologic Unit I

Sections 125-783A-1R-1, 0 cm, to 125-783A-14R-1, 12 cm; depth, 120.0 mbsf.

Age: middle or early Pleistocene to early Pliocene(?).

Lithologic Unit I has varying amounts of silt-sized detritus, most of which represents a volcanic influx: glass (7%-58%), feldspar (trace-15%), pyroxene (0%-2%), chlorite (0%-2%), and epidote (0%-7%). A trace to 5% zeolite present in a few cores (Cores 125-783A-1R, 125-783A-3R through 125-783A-5R, 125-783A-7R, 125-783A-11R, and 125-783A-12R) is interpreted as an alteration product of volcanic glass.

The ash layers in Cores 125-783A-1R, 125-783A-4R, 125-783A-5R, and 125-783A-10R of Unit I all have sharp basal contacts, are 1 to 2 cm thick, and are composed of volcanic glass (60%-90%) and feldspar (5%-10%), variable amounts of pyroxene (as much as 15%), opaque minerals (as much as 5%), chlorite (trace amounts), and clays (as much as 15%). In addition to the ash layers are a few layers of vitric sands and silts with large admixtures of clay (30%-60%) that are interpreted as reworked ash.

Pumice, in millimeter- to centimeter-sized clasts, is scattered throughout the unit. The pumice is usually located several centimeters above an ash layer and may be related to the same eruptive event as the underlying ash layer, with the pumice requiring a longer time for gravitational settling through the water column than the smaller vitric fragments.

Lithic fragments, such as marlstone and claystone, were observed in Cores 125-783A-1R, 125-783A-4R, and 125-783A-5R. Thulite, which was commonly observed in association with serpentine at Site 780 (see "Lithostratigraphy" section, "Site 780" chapter, this volume), occurs in Cores 125-783A-4R, 125-783A-5R, and 125-783A-8R. Serpentine was also observed (in Cores 125-783A-5R, 125-783A-7R, 125-783A-8R, 125-783A-10R, 125-783A-12R, and 125-783A-14R) and increases downhole from trace amounts to 10%.

Lithologic Unit I contains a small biogenic contribution: spicules (as much as 10%), radiolarians (as much as 5%), diatoms (as much as 10%), silicoflagellates (rarely present, a trace amount to 1%), nannofossils (rarely present, as much as 15%), and foraminifers (rarely present, 3%-4%). Parts of the unit have sufficient biogenic constituents to be nannofossil-bearing or -rich, or biogenic silica-rich. Calcareous biogenic material is lacking in the lower section of this unit, whereas siliceous biogenic material is present throughout the section. Diatoms are present from the top of the unit down to at least Section 125-783A-10R-CC, and radiolarians occur throughout the section, including the base of Unit I in Core 125-783A-14R.

Nannofossils present in Sample 125-783A-1R-1, 1 cm, from the top of the first core, provide a stratigraphic age of middle or early Pleistocene for the uppermost sediment in Unit I. Section 125-783A-10R-CC, near the base of the unit, has a diatom biostratigraphic age of early Pliocene; the age of the oldest stratum in Unit I is unknown but is at least early Pliocene.

Table 2. Lithologic units recovered at Site 783, Leg 125.

Lithologic unit	Cores	Depth (mbsf)	Dominant lithology	Stratigraphic age
I	783A-1R-1, 0 cm, to 783A-14R-1, 12 cm	0.0–120.0	Vitric clayey silt, glass-rich silty clay/claystone	middle or early Pleistocene to early Pliocene(?)
II	783A-14R-1, 12 cm, to 783A-18R-1, 147 cm	120.0–158.6	Phacoidal sheared serpentinite with vertical convolute bedding	?

The change from clay to claystone is typical of burial diagenesis. The clay gradually is compacted, becomes firmer, and eventually is sufficiently lithified in parts of the core so that it becomes necessary to cut the core with a saw to minimize disruption of the sediments. The transition from clay to claystone occurs in Section 125-783A-8R-1. In addition to the burial diagenesis, there is an apparent overprint of tectonic diagenesis beginning in Section 125-783A-8R-2, 130 cm, and continuing into Section 125-783A-8R-3. This is seen as a scaly fabric with slickensided surfaces of claystone and the development of a spongy texture with higher apparent permeability than the overlying claystone (for further discussion see "Structural Studies" section, this chapter). The sediment in this region may have provided a pathway for fluids to escape from the underlying serpentinite in lithologic Unit II.

Lithologic Unit II

Sections 125-783A-14R-1, 12 cm, to 125-783A-18R-1, 147 cm; depth, 120.0–158.6 mbsf.

Age: ?

The contact between lithologic Units I and II was not recovered. The immediate interval is represented by serpentinite-bearing, feldspar- and glass-rich silty clay underlain by a 1-cm interval of volcanic ash, which is disseminated along the core liner for the next 4 cm (a 4-cm void in the core), followed by a 2-cm-diameter clast of serpentinitized ultramafic rock. Lithologic Unit II is composed of phacoidal sheared serpentinite that displays convolute bedding and blocks of serpentinitized harzburgite; in Core 125-783A-18R the composition is primarily blocks of serpentinitized harzburgite with some matrix of phacoidal sheared serpentinite.

No fossils or obvious detrital components were found in this unit. The age of these strata is unknown. In the absence of evidence for faulting, it is likely that this unit is in stratigraphic continuity with Unit I, in which case Unit II is probably at least early Pliocene, the oldest diatom biostratigraphic age in the overlying unit.

BIOSTRATIGRAPHY

Calcareous nannofossil and diatom evidence from Site 783 indicates that the sedimentary interval from Samples 125-783A-1R-1, 28 cm, to 125-783A-10R-CC ranges in age from middle to early Pleistocene to the early Pliocene. No ages could be assigned to the remaining sedimentary cores (125-783A-11R to 125-783A-15R).

The sedimentary interval in Hole 783A may have been deposited near the carbonate compensation depth (CCD), as shown by strong dissolution of the calcareous plankton assemblages. Nannofossil evidence suggests that Sample 125-783A-13R-CC was probably reworked.

Calcareous Nannofossils

Samples from Cores 125-783A-1R, 125-783A-3R, 125-783A-4R, and 125-783A-13R contain rare to common, poor to moderately preserved nannofossil assemblages. The poor

preservation probably resulted from deposition at or near the CCD. Samples 125-783A-1R-1, 28 cm, 125-783A-3R-CC, and 125-783A-4R-CC can be given a generic middle/early Pleistocene age based upon the presence of rare *Pseudoemiliana lacunosa* and unidentified species of *Gephyrocapsa* sp. A common, moderately preserved assemblage in Sample 125-783A-4R-1, 69 cm, is recognized to have an early Pleistocene age corresponding to the "Small *Gephyrocapsa* Zone" (Gartner, 1977) within Zone CN14a.

A rare, well-preserved late Eocene nannofossil assemblage (Zones CP14b/15) containing *Dictyococcites bisectus*, *Sphenolithus predistentus*, *Discoaster barbadiensis*, and *Cribrocentrum reticulatum*, together with dissolved fragments of coccoliths that appear to be younger in age, is present in Sample 125-783A-13R-CC. The good preservation and rarity of the Eocene nannofossils (usually well-preserved Eocene assemblages are abundant) suggest reworking.

Foraminifers

No samples examined from Site 783 (Samples 125-783A-1R-CC to 125-783A-15R-CC) contained planktonic or benthic foraminifers. This is probably because deposition took place at or below the CCD.

Diatoms

Rare to common, poorly preserved to well-preserved diatom assemblages are present in the sedimentary interval at Hole 783A. In the majority of the samples, however, fragments (of *Thalassionema nitzschioides* and some *Ethmodiscus rex*) dominate. Therefore, it was only possible to date three samples.

Sample 125-783A-1R-CC is characterized by *Pseudoeunotia doliolus* and *Nitzschia reinholdii*. Sample 125-783A-1R-1, 1 cm, also contains *N. reinholdii*, assigning the whole of this core to the lower Pleistocene (*N. reinholdii* Zone).

Sample 125-783A-5R-CC was dated as late Pliocene by the presence of *Rhizosolenia praebergonii* and the absence of *P. doliolus* (*R. praebergonii* Zone).

Nitzschia jouseae is present in Sample 125-783A-10R-CC; therefore, this sample is early Pliocene in age.

IGNEOUS AND METAMORPHIC PETROLOGY

The rocks recovered from Site 783 are serpentinitized harzburgite (90%–95%), dunite (5%–10%), and subordinate metabasalt and meta-volcaniclastic rocks. These form clasts of isolated fragments and occur as inclusions in a matrix of highly sheared and pulverized serpentinite. The clasts are 1 to 10 cm in diameter and subangular to subrounded in shape.

Ultramafic Rocks

Serpentinitized Harzburgite

The clasts of serpentinitized harzburgite are massive and dark bluish gray (5B 4/1) to black (5G 3/2). The primary mineralogy of the harzburgite is olivine (85%–90%), orthopy-

roxene (10%–15%), clinopyroxene (1%–2%), and chromium-spinel (trace–2%). Olivine is anhedral and 0.5 to 3 mm in size. Orthopyroxene is subhedral to anhedral and 1 to 5 mm in diameter. Clinopyroxene is present as blebs and anhedral crystals (less than 1 mm), closely related to orthopyroxene, and as exsolution lamellae (on [100]) in orthopyroxene. Chromium-spinel is dark red in color, 0.2 to 1 mm in diameter, and exhibits a subhedral to anhedral shape. Wavy extinction and rare kink-banding are recognizable in olivine, orthopyroxene, and clinopyroxene crystals.

One distinctive feature of Sections 125-783A-17R-CC and 125-783A-18R-1 is the presence of 0.5- to 1.5-cm-thick pyroxene-rich lherzolitic bands within the harzburgite (Fig. 3). These contain olivine (60%–75%), orthopyroxene (15%–20%), clinopyroxene (5%–20%), and spinel (trace–2%). Orthopyroxene and olivine are anhedral, 1 to 4 and 1 to 3 mm in diameter, respectively. Clinopyroxene forms subhedral to anhedral crystals (1–2.5 mm) and exsolution lamellae (on [100]) in orthopyroxene. Spinel is subhedral to anhedral and 0.2 to 1 mm in diameter. Spinel is dark brown and probably low in chromium and high in aluminum. The contact between the band and the host rock is obscure.

Olivine and orthopyroxene are variably replaced by serpentine minerals, which appear to be mostly chrysotile and/or lizardite. A mesh texture after olivine is predominant, and undeformed bastite pseudomorphs of orthopyroxene are common. Clinopyroxene is less serpentinized. Anastomosing veins of serpentine can be seen in some clasts. The degree of serpentinization is variable, from 60% to 95%.

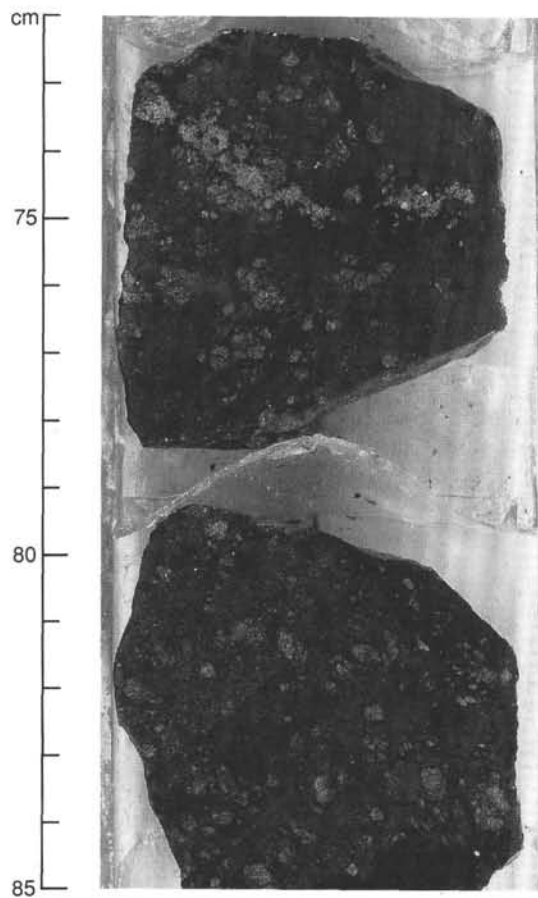


Figure 3. A pyroxene-rich (lherzolitic) band in the upper harzburgite clast in Section 125-783A-18R-1, 72–85 cm.

Serpentinized Dunite

Highly serpentinized (greater than 95% serpentine) dunites are rare. They are massive and black (5G 3/2) in color. The rocks consist of olivine (greater than 95%), orthopyroxene (less than 5%), and chromium-spinel (less than 1%). Serpentinized olivine exhibits a massive mesh-textured fabric, and there are rare, undeformed bastite pseudomorphs of orthopyroxene. Dark reddish chromium-spinel is well preserved.

Metavolcanic Rocks

Metabasalt

Several clasts of metabasalt, 1 to 1.5 cm in diameter, were recovered. Most of the clasts are grayish green (5G 4/2–5G 5/2), and one clast containing abundant limonite is dark reddish brown (5YR 2.5/2). The metabasalts are composed of plagioclase, clinopyroxene, olivine(?), and glass as primary phases and chlorite, albite, sphene, dusty brownish clay, zeolite, and limonite as secondary phases. The primary igneous textures, such as intersertal and aphyric textures, are well preserved, but almost all the primary minerals except clinopyroxene are fully chloritized. All of the clasts are fractured to varying degrees and contain 0.2- to 0.8-mm chlorite veins running throughout. Zeolite fills in vesicles greater than 0.2 mm.

Meta-Volcaniclastic Rock

Only one example of a clast of meta-volcaniclastic rock was recovered. The rock is 5 cm in diameter, light greenish-gray (5G 7/1), and medium- to fine-grained and consists of plagioclase and clinopyroxene as relic minerals and prehnite, aluminum-rich epidote, actinolite, chlorite, sphene, and probably hydrogrossular as secondary minerals. The clast contains abundant subangular to subrounded fragments of plagioclase and clinopyroxene within a fine-grained dusty matrix. The size of the fragments is variable, ranging from less than 0.1 to 1 mm. Most of the clinopyroxene fragments are altered to colorless actinolite, and those of plagioclase to aluminum-rich epidote and prehnite. The textural relationships suggest that prehnite, epidote, and actinolite are an equilibrium assemblage. Later-stage cataclastic deformation has developed along the boundaries of fragments.

IGNEOUS AND METAMORPHIC GEOCHEMISTRY

Five of the ultramafic clasts (harzburgites) from Site 783 were selected for shipboard geochemical analysis. Preparation and analytical techniques are given in the "Explanatory Notes" chapter of this volume. Rock and thin-section descriptions are given in the preceding "Igneous and Metamorphic Petrology" section. The geochemical data are listed in Tables 3 and 4.

Ultramafic Samples

Modal estimates of the original (pre-serpentinization) composition of ultramafic rocks range from 74% to 86% olivine, 12% to 20% orthopyroxene, 1% to 5% clinopyroxene, and less than 2% spinel. The degree of serpentinization of the samples varies from 55% to 92%.

Major-Element Chemistry

Loss on ignition (LOI) of these samples ranges from 12.62 to 15.75 wt% and like that of the samples from Site 779, shows a positive correlation with the degree of serpentinization (Fig. 4). (See "Igneous and Metamorphic Geochemistry" sections of "Site 778" and "Site 779" chapters, this volume, and "Explanatory Notes" for an explanation of LOI.) Concentra-

Table 3. Major-element data for serpentinized harzburgites from Hole 783A.

Core, section: Interval (cm):	16R-CC, 14-17	16R-CC, 19-22	17R-1, 9-12	18R-1, 49-51	18R-1, 96-97
SiO ₂	36.41	39.21	35.90	36.01	36.84
TiO ₂	0.00	0.00	0.00	0.00	0.00
Al ₂ O ₃	0.41	0.59	0.35	0.47	0.45
Fe ₂ O ₃	7.28	7.37	7.42	7.64	7.87
MnO	0.09	0.11	0.11	0.12	0.11
MgO	40.18	38.19	39.39	39.35	39.91
CaO	0.43	1.66	0.31	0.66	0.63
Na ₂ O	0.00	0.00	0.00	0.00	0.00
K ₂ O	0.00	0.00	0.00	0.00	0.00
P ₂ O ₅	0.00	0.00	0.00	0.00	0.00
NiO	0.28	0.25	0.29	0.30	0.29
Cr ₂ O ₃	0.16	0.21	0.18	0.21	0.25
^a LOI	14.83	12.62	15.75	14.99	13.55
Total	100.07	100.21	99.70	99.75	99.90
Mg#	91.62	91.12	91.32	91.07	90.94
^b %Serpentinization	70.00	55.00	92.00	60.00	60.00

Note: Data (in wt% oxides) from whole-rock analyses by XRF.

^a LOI = loss on ignition between 105° and 1030°C.

^b Estimated from thin sections.

tions of major-element oxides in these rocks are similar to concentrations in the harzburgites from Sites 778, 779, and 780. SiO₂ ranges from 35.90 to 39.21 wt%, MgO from 38.19 to 40.18 wt%, Al₂O₃ from 0.35 to 0.59 wt%, and Fe₂O₃ from 7.28 to 7.87 wt%. Magnesium number is also similar to that in the harzburgites from Sites 778, 779, and 780 and varies from 90.94 to 91.62. The concentrations of Na₂O, K₂O, and P₂O₅ are all below detection limits. The general absence of clinopyroxene crystals and very low concentrations of Al₂O₃ and CaO indicate that the rocks are residues from high degrees of partial melting.

Trace-Element Chemistry

In the trace-element data presented in Table 4, compatible elements are high in all samples, as would be expected. Values of chromium range from 1074 to 1716 ppm, and those of nickel, from 2210 to 2357 ppm, with the exception of low-nickel Sample 125-783A-16-CC (Piece 2, 19-22 cm), which contains 1980 ppm. Average concentrations of nickel in harzburgites from Sites 783 (2215 ppm) and 780 (2261 ppm) are slightly lower than those of the harzburgites from Sites 778 (2644 ppm) and 779 (2320 ppm). Chromium and nickel do not correlate with one another or with the degree of serpentinization.

Table 4. Trace-element data for serpentinized harzburgites from Hole 783A.

Core, section: Interval (cm):	16R-CC, 14-17	16R-CC, 19-22	17R-1, 9-12	18R-1, 49-51	18R-1, 96-97
Nb	tr	tr	tr	tr	tr
Zr	1	0	1	1	1
Y	nd	1	0	1	0
Sr	10	12	9	13	13
Rb	nd	nd	nd	0	nd
Zn	39	31	34	41	38
Cu	0	29	2	2	1
Ni	2210	1980	2267	2357	2260
Cr	1074	1469	1255	1451	1716
V	9	23	21	39	36
Ce	tr	tr	tr	12	tr
Ba	tr	tr	13	tr	15

Note: Data (in ppm) from whole-rock analyses by XRF; nd = none detected; tr = below detection limit (<5 ppm for Nb, <10 ppm for Ba and Ce).

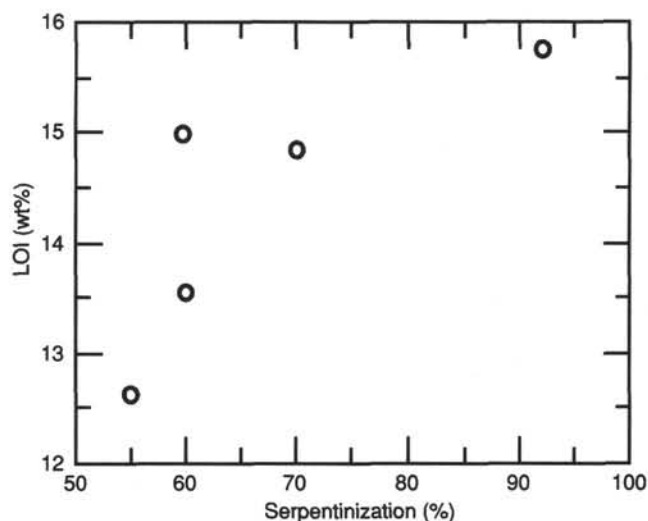


Figure 4. Modal percent of serpentinization vs. weight percent loss on ignition (LOI) of between 105° and 1030°C.

Niobium, zirconium, yttrium, rubidium, and titanium are all present in trace amounts or are below detection limits. Cerium and barium values range from below their detection limits (less than 10 ppm) to 12 and 15 ppm, respectively, although the cerium values at least may result from analytical error. Strontium varies from 9 to 13 ppm, similar to its concentrations in harzburgites from Sites 778, 779, and 780. Zinc ranges from 31 to 41 ppm, with an average concentration of 37 ppm, which is similar to that of the harzburgites from Site 780 (36 ppm) and slightly lower than those of harzburgites from Sites 778 (42 ppm) and 779 (39 ppm). There is no significant correlation between the geochemical parameters and depth.

Sample 125-783A-16R-CC (Piece 2, 19-22 cm) is anomalously rich in copper (29 ppm). It shows the highest concentrations of SiO₂ (39.21 wt%) and Al₂O₃ (0.59 wt%) of all the samples analyzed from this site. It also shows the highest concentration of CaO (1.66 wt%) and lowest nickel (1980 ppm) of all harzburgite samples analyzed from Sites 778 through 780 and 783. Note that this sample contains 5 modal% clinopyroxene (see "Igneous and Metamorphic Petrology" section) and represents the highest concentration of clinopyroxene in any analyzed sample. The petrogenetic implications are not clear, however, as the distribution of clinopyroxene indicates that this mineral was introduced by melt impregnation and was not a genuine residual phase. The hand sample appears to contain a 10-mm anhedral patch of a bronze-colored mineral that may be native copper or a copper sulfide.

In general, the samples analyzed from Site 783 are similar to those from Sites 778, 779, and 780 ("Igneous and Metamorphic Geochemistry" sections of the respective site chapters).

SEDIMENT/FLUID GEOCHEMISTRY

Sediment Geochemistry

Cores from Site 783 were analyzed aboard ship for inorganic carbon and for total carbon, nitrogen, and sulfur using the techniques described in the "Explanatory Notes" (this volume). The organic carbon content was then calculated by difference. These results are presented in Table 5 and Figure 5. The CaCO₃ content of the sediments and the phacoidal, sheared serpentine is extremely low, generally less than 1%, except for two intervals of sediment at 0 to 6 and 26 to 30

Table 5. Total nitrogen, carbon, inorganic carbon, organic carbon, and carbonate carbon in sediments and serpentine at Site 783.

Core, section, interval (cm)	Depth (mbsf)	Total nitrogen (wt%)	Total carbon (wt%)	Inorganic carbon (wt%)	Organic carbon (wt%)	CaCO ₃ (wt%)
119-783A-						
1R-1, 77-79	0.77			7.25		60.4
1R-2, 23-25	1.73			0.15		1.2
1R-3, 76-78	3.76	0.19	2.88	2.47	0.41	20.6
1R-4, 97-99	5.47			0.49		4.1
1R-5, 76-77	6.76			0.03		0.2
1R-6, 74-76	8.24			0.11		0.9
1R-7, 7-9	9.07			0.14		1.2
2R-1, 34-36	10.04			0.02		0.2
2R-2, 15-17	11.35	0.15	0.41	0.04	0.37	0.3
4R-1, 74-76	26.74			0.43		3.6
4R-2, 84-86	28.34			0.80		6.7
4R-3, 67-69	29.67	0.13	2.93	2.59	0.34	21.6
4R-4, 76-78	31.26			0.09		0.7
4R-5, 24-26	32.24			0.47		3.9
4R-CC, 8-10	32.61			0.06		0.5
5R-1, 56-58	36.26			0.09		0.7
5R-2, 62-64	37.82	0.18	0.54	0.04	0.50	0.3
5R-3, 40-42	39.10			0.02		0.2
5R-4, 25-27	40.45			0.03		0.2
5R-CC, 11-13	40.83			0.12		1.0
7R-1, 30-32	52.70			0.04		0.3
7R-2, 50-52	54.40			0.08		0.7
7R-3, 139-141	56.79	0.20	0.61	0.07	0.54	0.6
7R-4, 6-8	56.96			0.03		0.2
8R-1, 37-39	62.47			0.11		0.9
8R-2, 71-73	64.31	0.14	0.35	0.03	0.32	0.2
8R-3, 76-78	65.86			0.05		0.4
10R-1, 33-35	81.63			0.01		0.1
10R-2, 5-7	82.85	0.19	0.48	0.04	0.44	0.3
11R-1, 16-18	91.06	0.07	0.25	0.03	0.22	0.2
12R-1, 7-9	100.67	0.11	0.28	0.02	0.26	0.2
15R-1, 125-127	130.85			0.02		0.2
15R-2, 76-78	131.75	0.06	0.57	0.44	0.13	3.7
15R-3, 76-78	133.25			0.05		0.4
16R-1, 83-85	140.03			0.10		0.8
16R-2, 82-84	141.52	0.09	0.22	0.08	0.14	0.7
16R-CC, 5-7	142.89			0.07		0.6
17R-1, 127-129	150.17	nd	0.31	0.09	0.22	0.7
17R-CC, 10-12	150.50			0.10		0.8
18R-1, 82-84	159.42		0.18	0.05	0.13	0.4

Note: nd = not detected. Total sulfur was below the detection limit of 0.06 wt% in all samples analyzed for total carbon, nitrogen, and sulfur.

mbsf. The near-surface sediment interval contains up to 60 wt% CaCO₃, whereas the deeper interval contains up to 22 wt%. The organic carbon content decreases with depth from about 0.5 to 0.1 wt%. The nitrogen content varies with that of organic carbon, decreasing from 0.2 wt% to less than 0.01 wt% with depth. Sulfur is below the detection limit of 0.06 wt% in all samples.

Fluid Geochemistry

The concentration of methane measured for 5-cm³ headspace samples is uniformly low, less than 20 mL/L (Table 6). A single sample from 31 mbsf may have contained a trace of ethane. Other than this, methane was the only hydrocarbon detected.

The interstitial waters at Site 783 (Table 7 and Fig. 6) contrast markedly with those at Site 782 in response to the presence of serpentine at Site 783 at 120 to 158.6 mbsf. The serpentine consists of a matrix of phacoidal, sheared serpentine containing clasts of serpentinized harzburgite and metabasalt. It underlies 120 m of glass-rich silty clay to claystone. Between the lowest interstitial-water sample from the claystone at 83 mbsf and the highest from the serpentine at 131 mbsf, there are abrupt changes in pH, alkalinity, silica, sulfate, magnesium, calcium, sodium, potassium, and salinity. Only ammonia, chlorinity, and bromide are unaffected by the presence of the serpentine. Between the claystone and the serpentine, pH rises from 8 to almost 10, alkalinity decreases from 2.9 to 1.3 meq/kg, silica decreases from 643 to 2

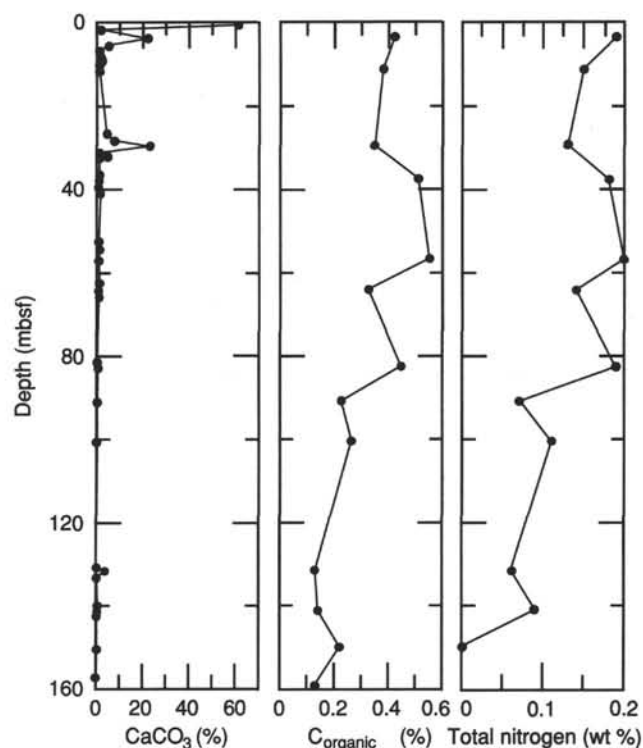


Figure 5. Weight percent of calcium carbonate, total organic carbon, and total nitrogen in sediments and serpentine at Site 783.

mmol/kg, and sulfate decreases from 28 to 6 mmol/kg. Magnesium decreases sharply from 50 to less than 1 mmol/kg, potassium decreases from 11 to 9 mmol/kg, calcium increases from 11 to 39 mmol/kg, and sodium increases from 480 to 499 mmol/kg, before decreasing again to 482 mmol/kg. Salinity decreases from 3.58 to 3.32 wt%, and chlorinity increases with depth within the claystone, probably as a result of the increased chlorinity of ocean bottom water during the Pleistocene glaciations (McDuff, 1985). It shows no further change within the serpentine. The decrease in salinity therein results from the decrease in sulfate.

The changes in pore-water composition between the claystone and serpentine almost certainly result from ongoing reactions between seawater-derived solutions and the partially serpentinized peridotite. Some of the changes are similar

Table 6. Results of headspace-gas analyses of cores at Site 783.

Core, section, interval (cm)	Depth (mbsf)	Methane	
		(μL/L) ^a	(μM) ^b
125-783A-			
1R-6, 0-3	7.52	10	0.9
2R-2, 0-3	11.22	9	0.8
4R-4, 0-3	30.52	11	1.0
^c 7R-2, 0-3	53.92	13	1.2
8R-2, 0-3	63.62	15	1.3
10R-2, 137-140	82.69	13	1.2
16R-3, 0-3	142.21	13	1.2
17R-1, 149-150	150.40	15	1.3

^a Microliters of methane per liter of wet sediment or wet unconsolidated serpentine, assuming a sample volume of 4.2 cm³ of sediment or serpentine.

^b Micromoles of methane per liter of interstitial water, assuming a porosity of 50%.

^c Trace of ethane present.

Table 7. Composition of interstitial waters from cores at Site 783.

Sample number	Core, section, interval (cm)	Depth (mbsf)	Volume (mL)	Squeeze temperature (°C)	pH	Salinity		Chlorinity (mmol/kg)	Alkalinity (meq/kg)	Sulfate (mmol/kg)	Sodium (mmol/kg)	Potassium (mmol/kg)
						(R.I., %)	(calcium, %)					
Surface seawater (17 March 1989)												
IW-1	1R-1, 145-150	1.48	35	2	8.25	35.6	34.65	539.2	2.689	27.78	462.0	10.11
IW-2	1R-2, 145-150	2.98	41	1	7.72	35.4	35.00	543.6	3.781	27.31	468.2	10.67
IW-3	1R-5, 145-150	7.48	36	2	7.85	35.4	35.03	544.5	3.212	27.41	468.3	10.87
IW-4	4R-3, 140-150	30.45	73	2	7.95	35.4	35.35	547.5	3.334	28.20	473.1	11.61
IW-5	7R-1, 140-150	53.85	58	2	7.95	35.6	35.61	553.3	3.294	27.77	476.1	11.49
IW-6	10R-1, 140-150	82.75	35	2	8.18	35.9	35.51	552.3	3.768	27.11	474.4	11.56
IW-7	15R-2, 140-150	131.05	10	6	8.01	36.1	35.79	557.2	2.890	27.61	480.5	11.11
IW-8	16R-1, 135-150	140.63	10	7	8.53	33.8	33.99	554.3	1.274	11.54	498.1	9.12
IW-9	17R-1, 140-150	150.35	9	7	9.96	33.0	33.27	549.4	1.377	7.85	489.1	8.46
					9.49	33.9	33.35	555.2	1.449	6.06	481.8	8.63

to those found in the serpentine sediments and flows at Sites 778, 779, and 780 on Conical Seamount in the Mariana forearc. Interstitial waters from the Conical Seamount sites were interpreted as mixtures of solutions from three sources: (1) seawater that had reacted with ultramafic rocks, (2) seawater that had reacted with mafic rocks and sediments, and (3) low-chlorinity water from a deep source probably associated with dewatering of the subducted lithospheric slab (see "Sediment/Fluid Geochemistry" section, "Site 780" chapter). The deep source of low-chlorinity water predominated at Site 780 on the summit, whereas reacted seawater predominated on the seamount flank at Site 779 and especially Site 778.

Pore waters at Site 783 on the Izu-Bonin seamount resemble the pore waters at the Mariana seamount (Sites 778-780) in their downhole increase in pH and ammonia and their strong downhole depletions in magnesium and silica. Although the concentrations of ammonia, magnesium, and silica are comparable between the two seamounts, the pH is not as high at Site 783 as it is at the Conical Seamount sites, with the exception of Site 778. For other dissolved species, Site 783 resembles Site 779 and especially Site 778 on the flank much more than Site 780 on the summit. Whereas alkalinity increases from the seawater value at Sites 779 and 780, it decreases at Sites 778 and 783. Sulfate likewise increases at Site 780 and decreases slightly and then increases at Site 779, but decreases greatly at Sites 778 and 783. Calcium decreases at Sites 779 and 780, but increases at Sites 778 and 783. Sodium increases at Site 780, but increases at Sites 778, 779, and 783. Potassium increases at Site 780, but decreases at Sites 778, 779, and 783. Chlorinity falls at all three Conical Seamount sites, especially at the summit (Site 780), whereas it increases within the claystone at Site 783 and shows no further change within the serpentine. Methane is abundant at Sites 779 and 780, moderately abundant at Site 778, and nearly absent at Site 783. Ethane and propane are present at Sites 779 and 780, but are absent at Sites 778 and 783.

Comparison of the interstitial waters from serpentinite at Sites 778, 779, 780, and 783 supports interpretation of the Conical Seamount waters as mixtures from three sources, as previously summarized. Because the waters at Site 783 most closely resemble those at Site 778, it is likely that these two sites represent the clearest examples of seawater-harzburgite interaction at low temperature. The associated reactions can be inferred to consume H^+ , alkalinity, silica, sulfate, Mg^{2+} , and K^+ and to produce ammonia, Ca^{2+} , and Na^+ while conserving chlorinity. Although a small fraction of low-chlorinity, hydrocarbon-rich water from a deep source is present at Site 778 on Conical Seamount, there is no evidence for such water at Site 783 on the Izu-Bonin seamount.

STRUCTURAL STUDIES

Deformation observed at Site 783 includes (1) shear fabrics developed in poorly lithified muds and in sheared phacoidal serpentine; (2) a possible small fault in poorly lithified material; (3) high-temperature, pre-serpentinization fabrics in peridotites; and (4) lower temperature, post-serpentinization fabrics in serpentinite cobbles. We will discuss these in turn, and then briefly discuss the structural and tectonic significance of the rheological measurements made at this site.

Structures in Pelagic/Volcaniclastic Muds

We observed no tectonic structures within the unlithified sediment that makes up the upper 62 m of material recovered from Hole 783A. The first partially lithified sediment occurs in Section 125-783A-8R-1 (62.1 mbsf). Section 125-783A-8R-3 consists of claystone with several intervals containing weakly developed shear and fracture foliations. From 95 to 107 cm in this section, the foliation consists of at least three sets of shear planes spaced from less than 1 mm to about 3 mm apart. It was possible to measure the orientations of two of these sets; one set is approximately vertical, whereas the other dips approximately 60° . The three sets of shear planes divide the siltstone into angular phacoids, or lozenges, the long axes of which define the macroscopically obvious foliation (Fig. 7). Between 113 and 120 cm is a "columnar" cleavage that consists of vertical fracture planes spaced from less than 1 to perhaps 3 mm apart. This foliation may be related to the presence of the small normal(?) fault described in the following text. Between 120 and 129 cm, the bottom of the section, the siltstone contains a lozenge foliation similar to that described for the interval between 95 and 107 cm, but this lower interval is difficult to study because it is shattered by drilling.

Two small faults cut the partially lithified claystone in the lower part of Section 125-783A-8R-3, one in the upper part of the interval containing the vertical ("columnar") fracture cleavage and one below it (Fig. 7). The upper fault sharply truncates a silty clay or claystone clast, dips about 40° , and flattens downward. Although the nature of the fault is unclear, its sharpness and the lack of anastomosing fault strands, associated gouge or breccia, or drag features suggest that its displacement is quite small, perhaps only a few centimeters.

The abrupt appearance of these brittle strain features (fracture and microfault foliations and small faults) shortly below the first visible lithification suggests that the greater cohesion of the lithified sediment facilitates brittle failure. Thus, diagenetic effects, including overburden pressure, probably determine the interval in which the structures are formed. However, overburden stress is probably not responsible for

Table 7 (continued).

Calcium (mmol/ kg)	Magnesium (mmol/kg)	Bromide (mmol/ kg)	Silica (μ mol/ kg)	Ammonia (μ mol/kg)
10.18	52.48	0.81	0	10
10.51	51.04	0.89	471	7
10.53	51.18	0.75	503	10
10.69	50.54	0.87	526	103
10.80	51.46	0.85	643	70
11.13	51.04	0.79	654	94
11.39	50.47	0.77	643	120
29.47	6.24	0.84	17	188
34.00	0.45	0.84	2	151
39.21	0.00	0.89	4	125

the foliations or the small faults. The former indicate a greatest principal stress oriented at 15° or more from vertical; the latter indicate horizontal extension that might accompany larger-scale faulting or slumping of adjoining sediment, but would probably not take place at such a small scale during normal compaction in the absence of tectonism. We do not have sufficient data to demonstrate the origin of these structures, but suggest the following: (1) all the structures may be related to large-scale basement faulting (compressional or extensional) in the forearc; (2) the normal(?) faults may have formed during lateral extension allowed by the slumping of material downslope from the hole; and (3) all the structures may have formed in response to stresses

exerted by the continuing downhill creep of the underlying serpentine sediments and flows.

Structures in Serpentine Sediments and Flows (Flow Matrix)

The material recovered in Cores 125-783A-15R through 125-783A-18R consists of a matrix of sheared phacoidal serpentine that bears fine-sand- to cobble-sized clasts, largely of serpentinized harzburgite tectonite (Fig. 8). The matrix exhibits a spectacular anastomosing shear foliation defined by deformed color banding (light blue to light blue-green to light green to pale yellow-green) and by the long axes of phacoidal (lens- or pie-shaped) serpentinite fragments. The shear foliation is always parallel to the layering defined by color banding and variations in clast size and concentration. Axial-plane foliations are not observed.

The phacoids are from 1 to 12 cm long and from a few millimeters to a few centimeters across (Fig. 8, 124–127 cm, and Fig. 9). Close inspection shows that much of the material between large phacoids consists of smaller phacoids. The foliation is whorled, contorted, and convolute with foliation streams swirling, branching, and rejoining around the larger clasts. Scattered through the material are smaller, angular to subangular and, less commonly, subrounded, sand- to small-pebble-sized clasts of serpentinite. Although some of these are light green, many are dark green to dark blue-gray; because

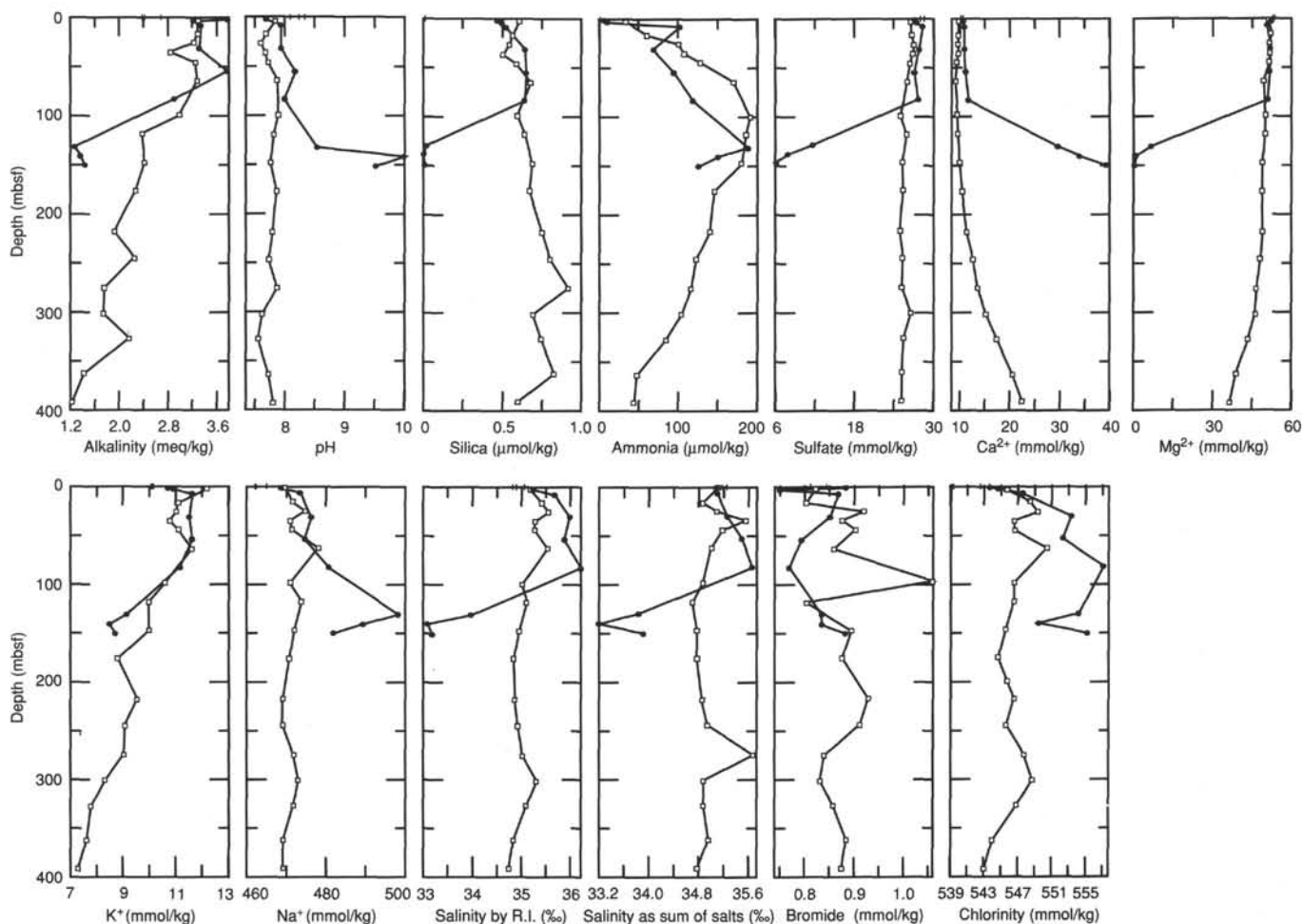


Figure 6. Composition of interstitial waters from sediments at Site 783 (circles) compared with that from Site 782 (squares) and surface seawater collected 22 February and 4 and 17 March 1989 (crosses).

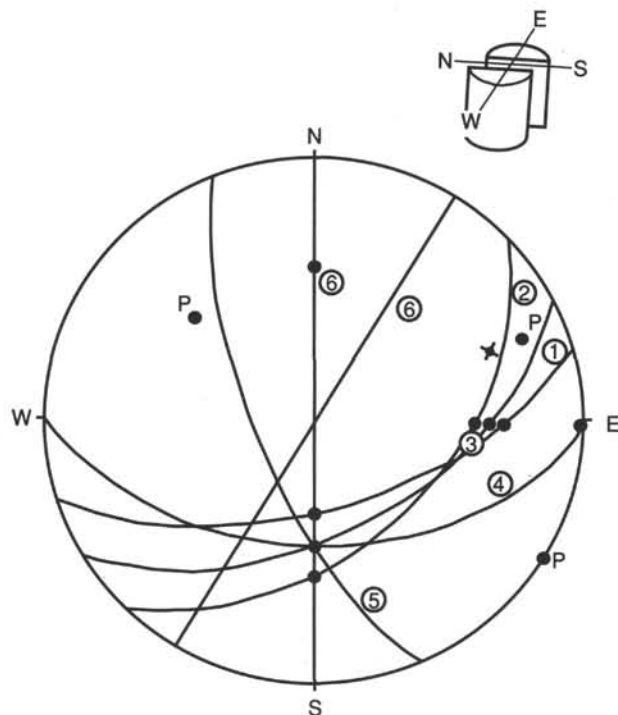


Figure 7. Stereonet showing the orientations of fractures that define shear foliation in Section 125-783A-8R-3, 95–107 cm. 1, 2, and 3 = faults with displacement; 3 is a normal fault. 4, 5, and 6 = cleavage planes. P = pole of plane.

their concentration varies greatly from one layer to the next, they help to define the foliation (Fig. 9).

Phacoids within the matrix typically exhibit pinch-and-swell texture (boudinage) along their long axes and commonly are cut by serpentine veins and/or microfaults at high to moderate angles with respect to their long axes. These microfaults almost universally show a normal sense of movement with respect to the long axes of the phacoids (Fig. 8, 124–127 cm, and Fig. 10, especially between 75 and 77 cm and between 83 and 85 cm). This texture, together with the boudinage and veining, clearly indicates that the phacoidal matrix has undergone major extension (pure shear) parallel to the layering, foliation, and the direction of alignment of the phacoids. This extension was both brittle and ductile, the difference presumably depending on confining stress, strain rate, and the degree of lithification and water content of phacoids and interphacoid matrix.

The phacoids are commonly bounded, and their tapering ends terminated, by shear bands (zones in which the bulk shear is concentrated) within the surrounding finer-grained matrix. Phacoids that lie parallel to the local direction of the matrix foliation are typically lensoid (i.e., their long axes are straight). Phacoids that are oblique to the surrounding foliation are typically sigmoid, with their long axes bent and their ends sheared out parallel to the foliation. Pure and simple shear have thus both played an important part in forming the fabric. Shear bands may extend across the entire core or die out within the matrix. Therefore, the overall geometry of matrix foliation and phacoid alignment outlines the pattern of matrix streamlines, along which extensional flow has occurred.

Although we have not yet measured the orientation of the shear foliation in detail, we observe no strong preferred orientation. Whorled foliation, in which the whorls appear to have long vertical limbs, appears to dominate some parts of

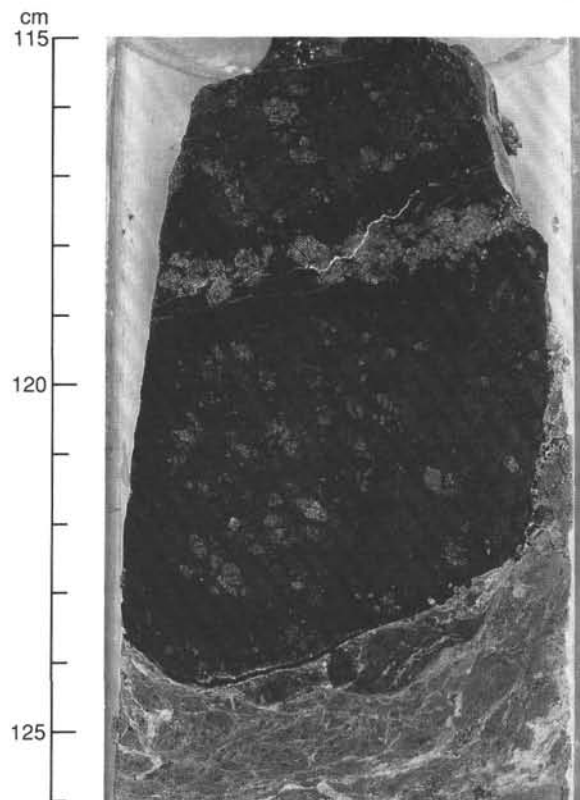


Figure 8. Sheared, phacoidal serpentine matrix enclosing serpentized harzburgite tectonite clast (Section 125-783A-18R-1, 115–126 cm).

the cores. This texture, described elsewhere in this chapter as “vertical convolute lamination,” is probably an artifact of the aspect ratios of our core sections, which are 150 cm long and 6.5 cm wide; fabrics parallel to the core will thus appear to dominate the geometry.

We interpret these textures as flow fabrics developed in sheared serpentinite as it continued to hydrate, soften, and flow downhill under the influence of gravity. Although we believe that the original shearing of the serpentinite was tectonic in the sense that it was caused by deep-earth processes, we suggest that these near-surface processes formed much of the present fabric of the rock.

High-Temperature Peridotite Deformation Textures

Clasts larger than 1 cm, mostly of serpentized harzburgite tectonite, were encountered from Section 125-783A-15R-1, 15 cm, through the bottom of Core 125-783A-18R, but are dominant only in Core 125-783-18R, where they make up about 80% of the material recovered. These clasts preserve some relict mineralogy, but the specimens from which our thin sections were made have been so highly serpentized that relict textures developed at depth under elevated pressure and temperature could not be observed. Deformation textures observed in similar clasts from Sites 778, 779, and 780 include subgrain bands and deformation lamellae in olivine, kink-bands in orthopyroxene, and undulatory extinction in both.

Serpentinization Textures

The serpentinization textures in clasts are similar to those observed in clasts from Sites 778, 779, and 780 and include serpentinization veins, cross-fiber serpentine veins, and “Frankenstein” veins (see “Structural Studies” sections in “Site 779” and “Site 780” chapters, this volume). A spectac-

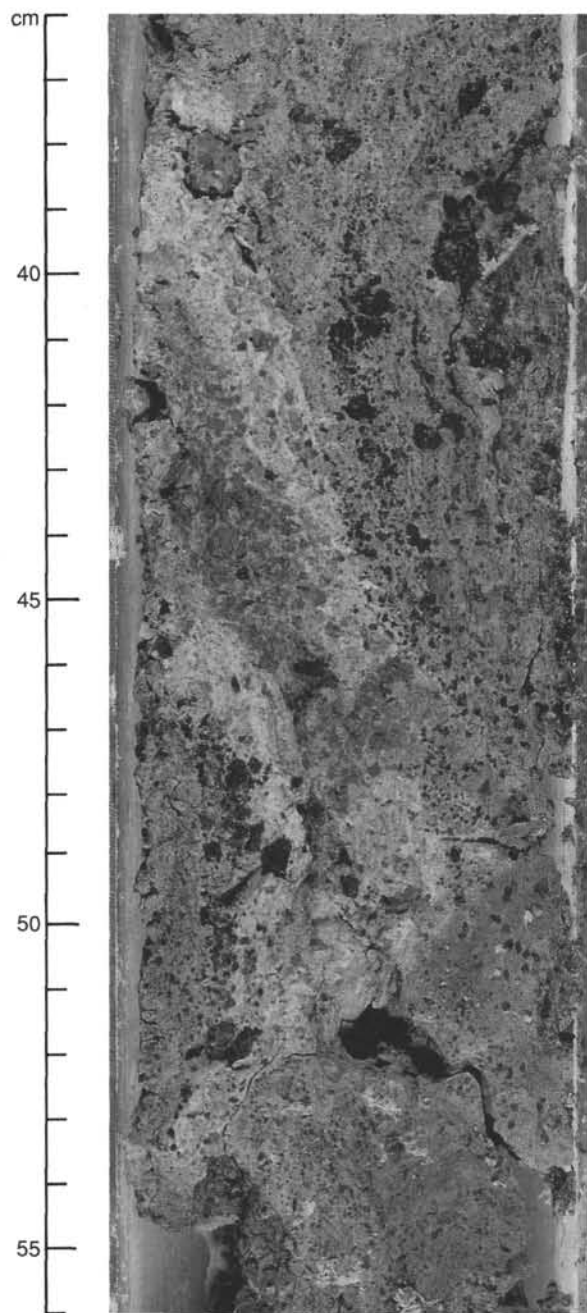


Figure 9. Layering, shear foliation, and phacoids in serpentinite sediments and flows (Section 125-783A-15R-2, 36–56 cm).

ular dark serpentinization vein with an unusual light center is shown in the large clast in Figure 8. The upper edge of the larger clast from 116 to 124 cm in Section 125-783A-18R-1 is bounded by a small, poorly developed “Frankenstein” vein. Textures seen in thin section include cross-fiber veins and fiber haloes surrounding relict and pseudomorphed olivine subgrains.

Many fiber haloes in serpentinized harzburgites from Site 783 are asymmetric, in striking contrast to those from Site 780, which are almost all highly symmetric (see Fig. 7). While detailed study will be necessary to confirm and quantify this observation, it probably implies that many of the Site 783 harzburgites were serpentinized in anisotropic stress fields (i.e., under deviatoric stresses).

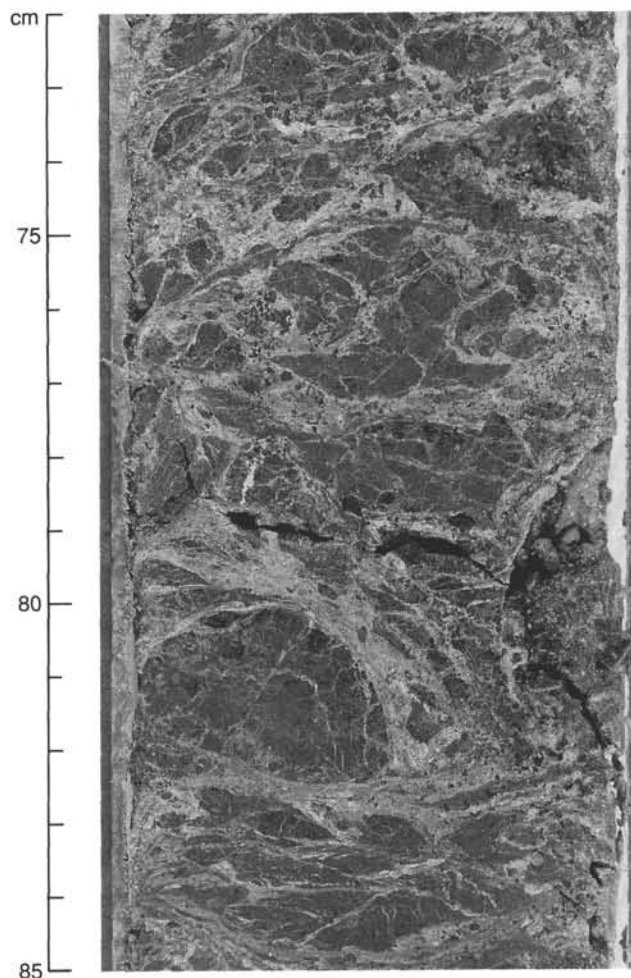


Figure 10. Normal microfaults, boudinage, and veining (evidence of layer-parallel extension) in phacoidal serpentinite. The interval shown (Section 125-783A-16R-1, 72–85 cm) probably represents a single serpentinite clast that is being softened by continuing hydration, disaggregated, and sheared out into the matrix.

Important vein textures are developed in the sheared serpentinite. Section 125-783A-14R-1, 10–20 cm, preserves much of the contact between more “normal” pelagic/volcaniclastic sediment, containing about 4 modal% serpentine, and the underlying serpentinite. Section 125-783A-14R-1, 13–15 cm, is a serpentinized harzburgite tectonite clast; the interval from 15 to 20 cm is unfoliated serpentinite sediment that contains a well-developed, branching network of cross-fiber serpentine veins up to 3 mm across that are clearly growing in the material. This is important because it provides unambiguous evidence that serpentinization is continuing in the disaggregated, unlithified sediment.

Within the sheared phacoidal serpentinites below this level, both phacoid and interphacoid material are highly veined with serpentine. Although some veins in phacoids end at the phacoid margin, others pass outward into the matrix. Many of these veins have become deformed by, drawn out into, and incorporated within the matrix. Moreover, in at least two intervals (76–85 and 100–125 cm in Section 125-783A-16R-1) large serpentinite clasts are cut by intricate, anastomosing networks of veins, which pass out into narrow channels of finely phacoidal, serpentinite matrix that also cut the clasts (Fig. 10). The clasts were quite soft and water saturated when recovered. We postulate that

these intervals preserve in place a late stage of the fragmentation of large clasts by serpentine veins, their continuing hydration and softening, and their shearing and incorporation into the phacoidal matrix.

Inspection under the binocular microscope shows that the matrix consists of slickensided lenses of serpentine that, in turn, consist of smaller scales and lenses; adding water to this material and agitating it gently with a probe causes it to disaggregate completely into submillimeter-sized serpentine fragments, interspersed with which are subangular to sub-rounded sand-sized grains of serpentine. We suggest that the fragility of the matrix is a consequence of its hydration.

Rheologic Properties of the Materials and Structural and Tectonic Implications

We used a Wykeham-Farrance torsion-vane apparatus to perform stress-strain tests on the unlithified materials recovered from Site 783. The sheared phacoidal, serpentine matrix is weak, with failure strengths that range between 7.3 and 51 kPa and average 23 kPa. These materials are comparable in strength to similar materials recovered from other sites, although they are significantly weaker than the overlying claystones and significantly stronger than the average unfoliated serpentine at Site 780 (Table 8). Moreover, the mode of failure was quite different: at low strains, the stress-strain curves were much more linear, and the strain appeared to be more elastic. Moreover, the material failed in a brittle manner, by cracking, rather than yielding plastically at an ultimate strength (Fig. 11).

We interpret these results as the consequence of the greater dewatering and compaction of these materials than those studied previously on Conical Seamount. This conclusion is compatible with the nature of the material, which is quite different from the pasty, weak, plastic, little-foliated

serpentine sediment and flows recovered from the shallow levels of Sites 778 and 779 on the flanks of Conical Seamount. We have interpreted this pasty material as representing young serpentine debris flows that have only begun to dewater. At Site 783, pasty, unfoliated serpentine is restricted to Core 125-783A-14R, at the volcanogenic sediment/serpentine interface, which is likely to be a zone of extensive fluid transfer and is clearly a zone of active serpentinization. The sheared, phacoidal serpentine from Site 783 is also different from the unfoliated serpentine material from Site 780, which we postulate to be a site of active upwelling of water-charged mud. Our interpretation is also compatible with the similarity between the material from Site 783 and that from deep levels at Sites 778 and 779, which we think represent older debris flows that have undergone extensive dewatering. Finally, our interpretation is compatible with the location of the serpentine 60 m below the level at which the volcanogenic sediments may have first lithified.

The serpentine at Site 783 is blanketed by virtually serpentine-free sediment that is at least as old as early Pliocene. Thus, the stratigraphy, sedimentology, paleontology, and rheology of the materials recovered from Site 783 are all consistent with a scenario in which serpentinite debris-flow processes were once active on Torishima Forearc Seamount but have since ceased, allowing the serpentine and serpentinite to be blanketed with pelagic and volcanogenic sediment. Serpentinization and dewatering have, however, continued until the present.

PALEOMAGNETISM

Magnetic Remanence

The natural remanent magnetization (NRM) of the sediments contained within the archive halves of Cores 125-783A-1R, 125-783A-2R, 125-783A-4R, 125-783A-5R, 125-783A-7R, 125-783A-8R, and 125-783A-10R was measured using the cryogenic magnetometer. Intensities vary typically between 10 and 100 mA/m, but there is no trend in these values downhole. Cores were then demagnetized at 10 mT, which reduced the intensity typically by 10% to 20%. Addi-

Table 8. Ultimate strength of serpentine sediments and flows recovered at Site 783.

Core, section	Depth (mbsf)	Stress (kPa)
119-783A-		
1R-1	0.73	13.1
1R-3	3.70	37.1
1R-5	6.68	29.1
2R-1	10.93	17.5
2R-2	11.32	44.4
4R-2	28.16	34.9
4R-4	31.22	41.5
5R-1	36.56	32.8
5R-3	39.56	52.4
7R-1	53.44	29.8
7R-3	56.28	69.2
8R-1	62.97	34.9
15R-1	130.41	16.0
15R-1	130.83	51.0
15R-2	131.87	16.7
15R-3	133.33	35.7
16R-1	139.92	19.7
16R-2	141.92	25.5
16R-3	142.39	26.9
17R-1	149.97	41.5
Sediment		
Average		36.39
Standard deviation		14.88
Maximum		69.20
Minimum		13.10
Serpentine		
Average		29.13
Standard deviation		12.58
Maximum		51.00
Minimum		16.00

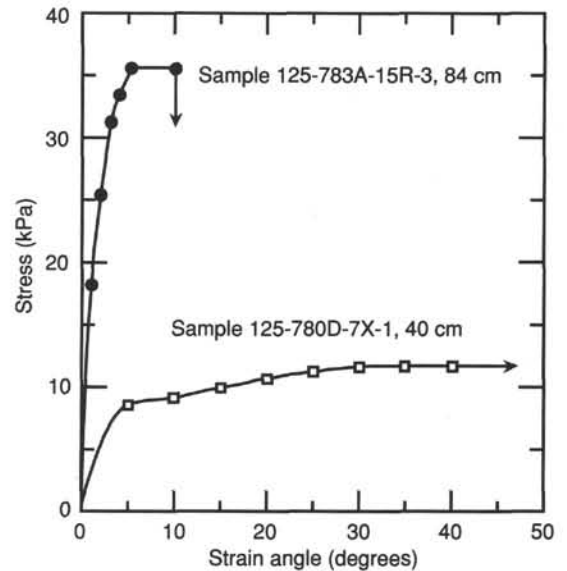


Figure 11. A representative stress-strain test of serpentine sediments and flows from Site 783 (failure strength = 35.7 kPa), compared with material from Site 780 on the summit of Conical Seamount (ultimate strength = 11.7 kPa).

Table 9. Remanence data for the discrete samples taken from Hole 783A.

Core, section, top of interval (cm)	Natural remanent magnetization			Remanent magnetization						Polarity
	Declination (degrees)	Inclination (degrees)	Intensity (mA/m)	(10 mT)			(20 mT)			
				Declination (degrees)	Inclination (degrees)	Intensity (mA/m)	Declination (degrees)	Inclination (degrees)	Intensity (mA/m)	
119-783A-										
1R-1, 103	325.4	30.0	77.3	348.0	52.0	47.3	349.5	51.8	36.8	N
1R-2, 33	0.5	15.5	71.4	12.3	23.0	62.5	14.9	28.9	52.1	N
1R-3, 6	343.0	60.2	63.6	351.0	62.1	51.7	351.9	63.1	37.9	N
1R-4, 11	63.0	74.7	101.0	84.4	69.6	69.2	89.0	69.6	49.8	N
1R-5, 86	302.4	62.3	90.7	301.2	63.3	82.4	302.4	65.4	62.1	N
1R-6, 89	344.5	47.8	73.3	344.3	48.0	61.7	345.7	48.8	48.1	N
1R-7, 45	333.0	74.0	7.6	270.3	53.9	7.9	268.1	62.3	6.3	N
2R-1, 52	24.7	-54.2	32.7	5.5	-55.8	37.1	0.7	-56.6	33.1	R
2R-2, 3	252.1	-55.0	44.2	250.2	-51.9	45.8	251.0	-51.4	36.7	R
4R-1, 114	33.0	-48.0	25.7	29.4	-58.3	22.8	36.8	-52.4	17.5	R
4R-2, 113	227.7	28.5	14.6	34.1	19.0	33.4	41.9	6.8	2.6	R
4R-3, 113	220.2	-32.5	23.1	210.9	-33.0	20.3	210.2	-31.2	16.8	R
4R-4, 113	238.6	-79.1	34.5	236.7	-76.1	37.6	238.6	-74.2	28.9	R
4R-5, 40	92.0	-19.0	62.2	93.9	-23.8	57.0	95.7	-25.3	44.2	R
5R-1, 26	171.4	-82.9	47.3	87.9	-51.9	36.6	88.1	-53.1	30.4	R
5R-2, 26	190.9	-75.8	60.5	190.6	-63.8	70.9	190.7	-65.6	60.5	R
5R-3, 26	87.1	-51.7	99.2	89.7	-54.6	110.0	89.6	-51.2	80.7	R
5R-4, 13	262.2	-50.7	67.1	261.3	-53.0	69.5	254.4	-49.9	48.4	R
7R-1, 90	122.7	-67.7	68.9	120.3	-67.5	67.2	119.9	-67.0	53.6	R
7R-2, 90	110.5	-53.6	82.5	108.8	-53.6	77.2	107.9	-52.9	61.5	R
7R-3, 90	182.1	-64.3	84.6	179.5	-63.8	79.1	179.2	-64.4	62.9	R
7R-4, 3	339.0	-46.2	118.0	338.2	-46.6	112.0	338.7	-46.7	87.4	R
8R-1, 120	262.8	53.7	123.0	262.0	53.0	111.0	261.9	54.4	98.3	N
8R-2, 120	86.5	55.3	48.7	92.3	56.7	41.5	92.3	56.4	38.4	N
8R-3, 91	278.8	44.5	41.6	279.6	49.4	37.1	274.1	50.0	31.0	N

Table 10. The polarity of each sediment core from Hole 783A and the corresponding diatom and nannofossil zones.

Core	Polarity	Diatom zone	Nannofossil zone
119-783A-			
1R	N	<i>N. reinholdii</i>	CN14a
2R	R		
4R	R		CN14a (lower/middle part)
5R	R	<i>R. praebergonii</i>	
7R	R		
8R	N		
10R	?	<i>N. jouseae</i>	

tionally, one specimen was removed from the working half of each processed section for a more detailed analysis. The NRM of these specimens was also measured using the cryogenic magnetometer. Intensities vary typically between 50 and 80 mT. Each specimen was then demagnetized at 5, 10, 15, and 20 mT and remeasured between each step. Demagnetization reduced the intensity typically by 25% to 35% at the 20 mT step. The demagnetization data for the discrete specimens are summarized in Table 9. Only small changes in the remanence direction are observed between the 10 and 20 mT steps. This suggests that the 10-mT whole-core data can be used to make reliable polarity evaluations. The polarity of each core is summarized in Table 10. (No polarity transitions were recorded within any of the cores.)

Unfortunately, the biostratigraphic data, obtained almost entirely from core-catcher material (see "Biostratigraphy" section, this chapter), are poor. However, a biostratigraphic zonation, based primarily on diatoms, but also including two horizons dated using nannoplankton biomarkers, allows us to correlate tentatively the polarity sequence with the time scale of Berggren et al. (1985). Barron (1985) correlated the internationally recognized low-latitude diatom zones with the polarity time scale of Ness et al. (1980). At least for the

interval from 0 to 4 Ma, the age of each magnetochron boundary in that time scale is not much different from that presented in the time scale of Berggren et al. (1985). For practical purposes, the relative positions of the diatom zones of Barron (1985) can be transferred directly onto the time scale of Berggren et al. (1985). This modified scheme was adopted here.

The magnetostratigraphy of Hole 783A is summarized in Figure 12. We have been able to identify partial records of the Brunhes Normal Polarity Chron (Core 125-783A-1R) and the Matuyama Reverse Polarity Chron (Cores 125-783A-2R through 125-783A-7R). Core 125-783A-8R may record part of the Gauss Normal Polarity Chron.

The pelagic sediment/serpentine sediment contact was identified within Section 125-783A-14R-1. Cores 125-783A-15R through 125-783A-18R were processed in the cryogenic magnetometer at 0 and 10 mT. The serpentine material has an NRM intensity typically between 50 and 200 mA/m. Both Cores 125-783A-16R and 125-783A-17R carry normal polarity magnetizations. However, as the serpentine material is not pelagic sediment, we are unable to fit the magnetic polarity data from these cores into any geochronological framework.

Magnetic Susceptibility

Magnetic susceptibilities were measured on the multisensor track (MST). A downhole plot of these values for Hole 783A is presented in Figure 13. The sediments (between 0 and just past 100 mbsf) have values typically between 3×10^{-4} and 6×10^{-4} SI units, whereas the serpentine has values typically between 1×10^{-3} to 3×10^{-3} SI units. The high magnetic susceptibility (and NRM intensity) associated with the serpentine almost certainly results because magnetite is produced during the process of serpentinization. The serpentine typically contains on the order of 2% by volume of magnetite ("Igneous and Metamorphic Petrology" section, this chapter).

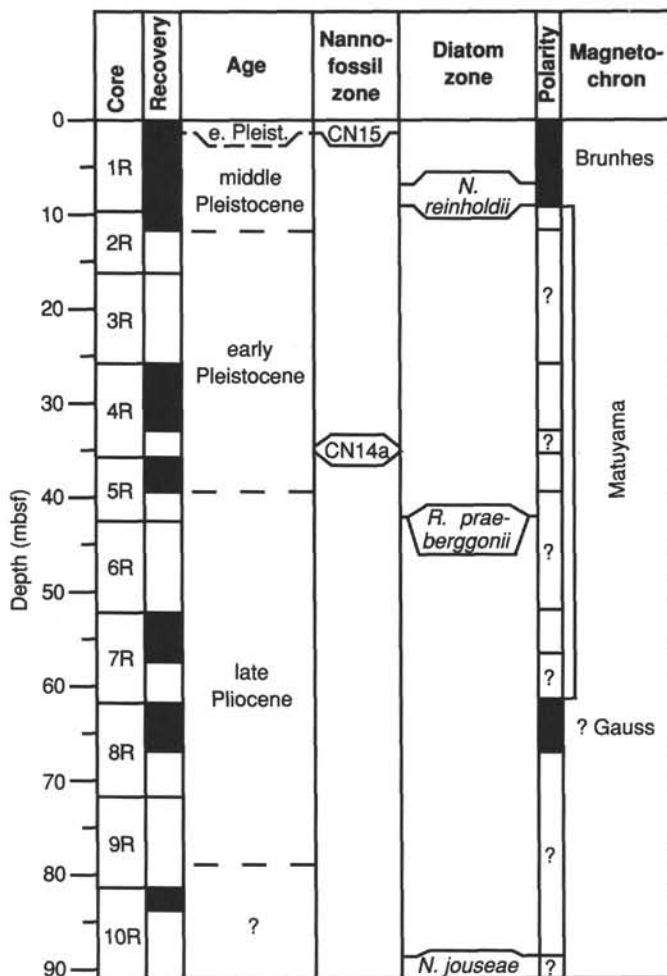


Figure 12. The magnetostratigraphy of Hole 783A (based on whole-core and discrete-sample data).

PHYSICAL PROPERTIES

The MST was used to determine bulk density (using the GRAPE), sonic velocity, and magnetic susceptibility in each core section from Hole 783A. Representative samples were selected from each section for measurement of bulk density, grain density, porosity, water content, and thermal conductivity. Where possible, shear strength, resistivity, and sonic velocity (using the Hamilton Frame device) were determined. Shear strength measured in material from this hole is reported in the "Structural Studies" section. Physical-property measurements are listed in Tables 11 and 12.

A total of 120 m of volcanoclastic and pelagic sediment was cored in Hole 783A. At about 120 mbsf, serpentine sediments and flows with dispersed hard-rock clasts were encountered. The physical properties of the volcanoclastic/pelagic and serpentine material in Hole 783A are distinct (Fig. 14). The separation between the volcanoclastic/pelagic and serpentine material can easily be seen between the two groups on the depth plot of the GRAPE-determined bulk-density data. The discontinuities in data points with depth are gaps in core recovery. The average bulk densities of the volcanoclastic/pelagic and serpentine material are $1.54 \pm 0.08 \text{ g/cm}^3$ and $2.01 \pm 0.19 \text{ g/cm}^3$, respectively. The P-wave logger, which is mounted on the MST, gave reliable compressional-wave sonic velocities for parts of the core from Hole 783A. Figure 15

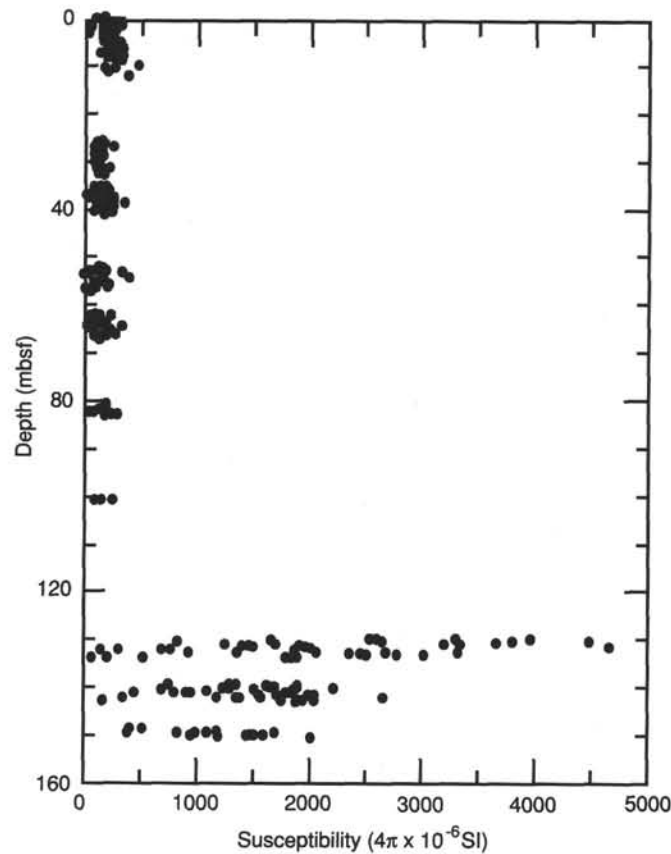


Figure 13. A downhole plot of magnetic susceptibility for Hole 783A.

illustrates how the velocities vary with depth; the average compressional-wave velocity is $1620 \pm 106 \text{ m/s}$ and is relatively constant over the depth range shown.

Table 11 lists the index properties of the discrete samples from Hole 783A. The bulk density of the volcanoclastic and pelagic sediment is relatively constant or decreases slightly to 100 mbsf (Fig. 16). At about 120 mbsf, where the serpentine material was encountered, the bulk density sharply increases. Values of bulk density of the serpentine material cluster around $2.14 \pm 0.03 \text{ g/cm}^3$ and show no obvious increase with depth. Although the values of grain density are scattered, their average is relatively constant with depth. The average grain densities of the volcanoclastic and pelagic sediment and serpentine material are $2.59 \pm 0.13 \text{ g/cm}^3$ and $2.71 \pm 0.13 \text{ g/cm}^3$, respectively.

The average thermal conductivity of sediment is $0.937 \pm 0.070 \text{ W/mK}$ (Table 11 and Fig. 16). At 120 mbsf, in the serpentine material, the thermal conductivity increases to 1.6 W/mK and rises steadily to 2.1 W/mK at 150 mbsf, resulting in a gradient of 0.029.

Measurements of sonic velocity were obtained from discrete samples of the serpentine material. The A velocities are measured parallel to the surface of the split core and the B velocities are measured perpendicular to the surface of the split core. With the exception of the harzburgite clast at 159 mbsf, the velocities are constant and isotropic with depth, with average A and B velocities of 194 and 196 m/s, respectively.

DOWNHOLE MEASUREMENTS

Two downhole temperature measurements were obtained at Site 783 using the Barnes-Uyeda temperature tool.

Table 11. Index properties for Hole 783A.

Core, section, interval (cm)	Depth (mbsf)	Bulk density (g/cm ³)	Grain density (g/cm ³)	Porosity (%)	Water content (%)	Void ratio
125-783A-						
1R-1, 77-79	0.77	1.47	2.58	72	52	0.72
1R-2, 23-25	1.73	1.48	2.69	73.2	52.5	0.73
1R-3, 76-78	3.76	1.5	2.73	72.9	51.7	0.73
1R-4, 97-99	5.47	1.46	2.56	72.4	52.8	0.72
1R-5, 76-78	6.76	1.48	2.59	71.3	51	0.71
1R-6, 74-76	8.24	1.49	2.52	69.2	49.2	0.69
1R-7, 7-9	9.07	1.4	2.54	71	53.9	0.71
2R-1, 33-35	10.03	1.42	2.18	66.2	49.4	0.66
2R-2, 15-17	11.35	1.55	2.91	72.6	49.7	0.73
4R-1, 65-67	26.74	1.5	2.59	70	49.5	0.7
4R-2, 84-86	28.34	1.47	2.62	72.4	52.2	0.72
4R-4, 76-79	31.26	1.49	2.63	71.7	51.2	0.72
4R-5, 24-26	32.24	1.52	2.6	69.1	48.3	0.69
4R-CC, 8-10	32.61	1.55	2.54	66	45.3	0.66
5R-1, 56-58	36.26	1.63	2.61	62.5	40.8	0.62
5R-2, 62-64	37.82	1.58	2.65	66.1	44.4	0.66
5R-3, 40-42	39.1	1.53	2.62	68.7	47.6	0.69
5R-4, 25-27	40.45	1.58	2.57	64.6	43.4	0.65
5R-CC, 11-13	40.83	1.54	2.6	68.2	47.1	0.68
7R-1, 30-32	52.7	1.54	2.4	63.3	43.7	0.63
7R-2, 50-52	54.4	1.58	2.64	66.4	44.7	0.66
7R-3, 139-140	56.79	1.58	2.45	61.8	41.6	0.62
7R-4, 6-8	56.96	1.59	2.58	64.4	43.1	0.64
8R-1, 37-39	62.47	1.49	2.42	67.3	48	0.67
8R-2, 71-73	64.31	1.55	2.53	65.5	44.9	0.66
8R-3, 76-78	65.86	1.52	2.41	64.9	45.4	0.65
10R-1, 33-35	81.63	1.5	2.64	70.8	50	0.71
10R-2, 5-7	82.85	1.48	2.68	71.5	51.2	0.72
11R-1, 16-18	91.06	1.62	2.59	62.6	41.1	0.63
12R-1, 7-9	100.67	1.44	2.54	73.2	54.1	0.73
15R-1, 125-127	130.85	2.1	2.67	34.6	17.5	0.35
15R-2, 76-78	131.75	2.15	2.61	29.5	14.6	0.29
15R-3, 76-78	133.25	2.16	2.84	38.1	18.8	0.38
16R-1, 83-85	140.03	2.07	2.57	32.4	16.6	0.32
16R-2, 82-84	141.52	2.11	2.66	34.2	17.2	0.34
16R-CC, 5-7	142.89	2.12	2.68	34.4	17.2	0.34
17R-1, 127-129	150.17	2.23	2.54	20.9	10	0.21
17R-CC, 10-12	150.5	2.17	2.58	26.5	13	0.26
18R-1, 82-84	159.42	2.56	2.57	0.4	0.2	0

The temperature record from Run 06R at 42.7 mbsf is shown in Figure 17A and at an expanded scale in Figure 17B. The probe was firmly seated in the sediment at 51 min into the run and remained relatively undisturbed until 66 min. After the first few minutes of emplacement, the temperature decay curve is proportional to 1/time. A linear least-squares regression on the curve, extrapolated to 1/time = 0, is a good estimate of the equilibrium sediment temperature, 3.29°C (Fig. 18). The correlation coefficient (r^2) has the somewhat low value of 0.527, but the slope of the regression line is negligible, so there should be no significant error.

The temperature record from Run 11R at 90.9 mbsf is shown in Figure 19A and at an expanded scale in Figure 19B. The probe was seated in the sediment from 55 to 66 min into the run, but the minor temperature increases at 59 and 63 min indicate slight disturbances to the probe. The equilibrium temperature of 3.93°C estimated from the decay curve (Fig. 20) has a low r^2 of only 0.334 because of the disturbances.

The temperature data must be combined with the thermal conductivity data ("Physical Properties" section; Fig. 21) to determine the heat flow at the site. Note that the large increase in thermal conductivity below 120 mbsf takes place below the depth of the temperature measurements from the two runs. The most useful way to analyze the temperature data is to plot temperature vs. the vertically integrated thermal resistivity. Thermal resistivity is simply the inverse of thermal conductivity. In the plot of integrated thermal resistivity vs. depth in Figure 22 the decreased slope of the line below 120 mbsf

results from the higher thermal conductivity of the deeper sediment.

The equilibrium temperature and integrated thermal resistivity data are plotted in Figure 23. The slope of the linear least-squares regression is the heat flow at this site, 23 mW/m². The quality of the fit is surprisingly poor.

Several factors might affect these data. The first is instrument performance, but that appears acceptable because the indicated temperature is similar in the bottom water before and after the penetration (Figs. 17 and 19). The second factor is a variation in bottom water temperature with time, but such a change would have to be extremely large, probably over 1°C. The bottom water temperature that we now observe is consistent with temperatures at similar depths in this region from the other temperature runs on this leg and from historic oceanographic data. The third factor is an exothermic chemical reaction in the sediment, but this is unlikely as the sediments were of an unexceptional nature. A fourth factor is slow advection of pore fluids upward through the sediments. If advection is occurring, the total heat flow at this site is higher than the least-squares estimate given here.

SUMMARY AND CONCLUSIONS

Site 783 (30°57.86'N, 141°47.27'E; water depth of 4648.8 m) is located on the northern, midflank part of a seamount that forms part of a 500-km-long ridge running along the lowermost, inner wall of the Izu-Bonin Trench. The single hole, 783A, attempted at this site was drilled to 168.2 mbsf with 27.9% recovery (Fig. 24). Heat-flow measurements were taken at 42.7 and 90 mbsf. Hole 783A was abandoned when the torque and pressure of the drill string suddenly increased.

Two lithologic units were defined as follows:

Unit I (0-120.0 mbsf) is middle or early Pleistocene to early Pliocene (or older) glass-rich silty clay to claystone;

Unit II (120.0-158.6 mbsf) is phacoidal, sheared serpentinite with clasts of serpentinitized harzburgite.

Dating is based on calcareous nannofossil and diatom biostratigraphy. Microfossil studies also indicate that the upper 100 m was deposited at or near the CCD and that reworking may have been important in places lower in the sequence. Lithologic Unit I as a whole has a small biogenic component, the siliceous biogenic contribution being greater than the calcareous contribution; it also has varying volcanic influx, primarily as glass with lesser amounts of feldspar, pyroxene, and amphibole.

The harzburgites of Unit II consist of olivine (80-90 modal%), orthopyroxene (10-15 modal%) with minor clinopyroxene (as exsolution lamellae in orthopyroxene), and spinel. Other rock types are very rare, although one piece of harzburgite contains a 5- to 15-mm-wide clinopyroxene-rich band and there are several small metabasaltic clasts. The degree of serpentinitization is variable, but rarely below 50%.

Deformation observed in the sediments at Site 783 begins with the first partially lithified sediment at 62.1 mbsf and includes shear fabrics and convolute plastic folding within the claystones of Unit I and the phacoidal serpentinite of Unit II. High-temperature pre-serpentinitization and lower temperature, post-serpentinitization fabrics similar to those described from Conical Seamount are found in the ultramafic clasts of Unit II.

Studies of physical properties show that the bulk densities increase from 1.47 to 1.590 g/cm³ in the sediments of Unit I and cluster about 2.1 g/cm³ in the serpentinite of Unit II. The average compressional-wave velocity in the sediments is 1.9 km/s. Thermal conductivities average about 1 W/mK in sediments and 1.91 W/mK in the serpentinite. Heat flow in the sediments is 23 mW/m².

Table 12. Physical properties for Hole 783A.

Core, section, interval (cm)	Depth (mbsf)	Thermal conductivity (W/mK)	Ultimate strength (kPa)	Resistivity (ohms)	Formation factor	Compressional-wave velocity	
						A direction (km/s)	B direction (km/s)
125-783A-							
1R-1, 76-80	0.75	0.888	13.1	10.8	1.26		
1R-2, 75	2.25	0.863					
1R-3, 76-80	3.75	0.939	37.1	11.2	1.31		
1R-4, 75	5.25	0.921					
1R-5, 76-80	6.75	0.98	29.1	11.4	1.33		
1R-6, 75	8.25	0.988					
1R-7, 6-10	9.08			11	1.28		
1R-7, 30	9.3	1.039					
2R-1, 30-34	10.02			12.5	1.46		
2R-1, 75	10.45	0.99					
2R-1, 123-125	10.93		17.5				
2R-2, 16-20	11.32	1.006	44.4	13.9	1.62		
2R-CC, 8	11.54	0.991					
4R-1, 60-64	26.62			16.3	1.9		
4R-1, 75	26.75	0.919					
4R-2, 75	28.25	0.925	34.9				
4R-3, 75	29.75	0.976					
4R-3, 86-90	29.88			15.4	1.8		
4R-4, 75	31.25	0.914	41.5				
4R-5, 20-24	32.26	0.994		15.4	1.8		
4R-CC, 7	32.6	0.989					
5R-1, 10-14	35.82			23	2.68		
5R-1, 75	36.45	0.955	32.8				
5R-2, 75	37.95	0.931					
5R-3, 10-14	38.82			18.5	2.16		
5R-3, 75	39.45	0.897	52.4				
5R-4, 24	40.44	0.912					
7R-1, 10-14	52.52			35.1	4.1		
7R-1, 60	53	0.998	29.8				
7R-2, 60	54.5	0.998					
7R-3, 10-14	55.52			20.1	2.35		
7R-3, 60	56	0.959					
7R-3, 88-90	56.28		69.2				
8R-1, 10-14	62.22			13.5	1.58		
8R-1, 67	62.77	1.004					
8R-1, 87-89	62.97		34.9				
8R-2, 67	64.27	0.906					
8R-3, 10-14	65.22			18.1	2.11		
8R-3, 67	65.77	0.833					
10R-1, 30-34	81.62			16.5	1.93		
10R-1, 58	81.88	0.9					
10R-2, 21	83.01	0.847					
11R-1, 12	91.02	0.682					
12R-1, 19	100.79	0.965					
14R-1, 15	120.05	1.624					
14R-CC, 8	120.22	0.638					
15R-1, 64-66	130.26			37	4.32		
15R-1, 75-81	130.35	1.123	16				
15R-1,	130.85		51			1.88	1.92
125-127							
15R-2, 54-56	131.66			91	10.62		
15R-2, 74-76	131.74	1.839	16.7			2.06	1.97
15R-3, 40-42	133.02			43	5.02		
15R-3, 74-76	133.24	1.961	35.7				1.98
15R-3, 87-91	133.49			100	11.67		
15R-CC, 4	134.03	1.606					
16R-1, 16-20	139.38			98	11.44		
16R-1, 75	139.95	1.94	19.7				
16R-1, 83-85	140.03					1.98	
16R-2, 80	141.5	1.827				1.86	
16R-2,	141.92		25.5				
122-124							
16R-3, 19-21	142.39		26.9				
16R-3, 30	142.5	1.348					
16R-3, 48-52	142.7			68.2	7.96		
16R-CC, 5-7	142.89					1.9	
16R-CC, 21	143.05	1.93					
17R-1, 30-34	149.22			45.7	5.33		
17R-1, 69	149.59	2.092					
17R-1,	149.97		41.5				
107-109							
18R-1, 80	159.4	2.322				5.62	5.76

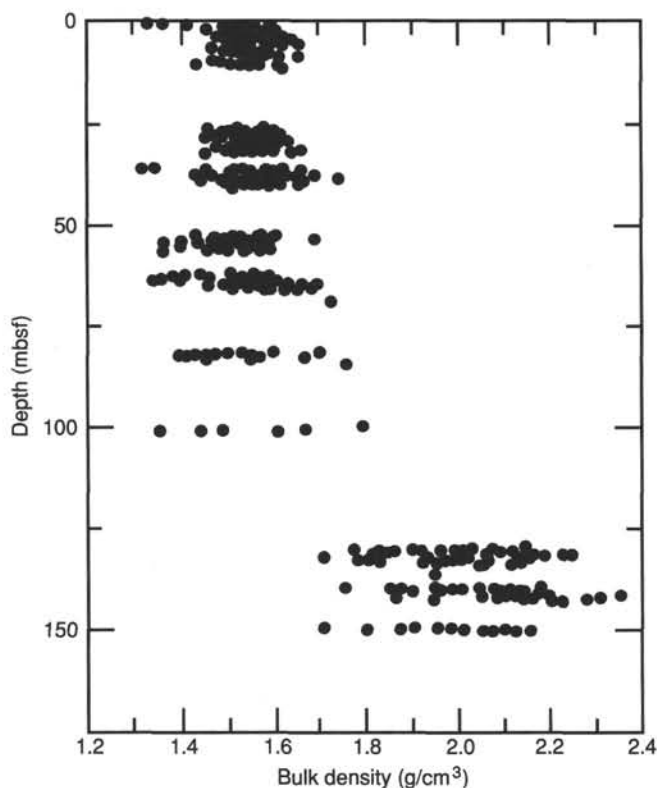


Figure 14. Bulk density (determined by the GRAPE) vs. depth for Hole 783A.

Interstitial-fluid compositions show only small variations with depth in the sediment, a sharp discontinuity at the claystone/serpentine boundary, and rapid chemical changes thereafter. Important variations with depth in the serpentine include an increase in pH from about 8 at the claystone/serpentine boundary to 9.5 to 10 at the bottom of the hole, a decrease in alkalinity (from about 3 to 1.3 meq/kg), depletions in silica (from 43 to 2

mmol/kg), magnesium (from 50 to mmol/kg), and sulfate (from 28 to 6 mmol/kg), increases in calcium (from 11 to 39 mmol/kg) and sodium (from 480 to 499 mmol/kg), decreases in potassium (from 11 to 9 mmol/kg) and salinity (from 3.59 to 3.32 wt%), and little change in ammonia, chlorinity, and bromide. Significant differences from the values measured at Conical Seamount are that calcium was depleted at Conical Seamount (by carbonate precipitation) and chlorinity decreased (possibly by mixing with deeper, fresher water).

The principal results of this site are (1) the confirmation that this seamount is made up, at least in part, of serpentine; (2) the biostratigraphic evidence that the serpentine sediment is at least early Pliocene in age and hence older than Conical Seamount in the Mariana forearc; (3) the structural evidence for deformation within the overlying sediments as well as within the serpentine; and (4) the evidence from fluid chemistry that serpentinization is still taking place, but without the low-chlorinity component identified at Conical Seamount (Sites 778-780).

REFERENCES

- Barron, J. A. 1985. Miocene to Holocene planktic diatoms. In Bolli, H., Saunders, J. B., and Perch-Nielsen, K. (Eds.), *Plankton Stratigraphy*: Cambridge (Cambridge Univ. Press), 763-810.
- Berggren, W. A., Kent, D. V., Flynn, J. J., and Van Couvering, J., 1985. Cenozoic geochronology. *Geol. Soc. Am. Bull.*, 96:1407-1418.
- Gartner, S., 1977. Calcareous nannofossil biostratigraphy and revised zonation of the Pleistocene. *Mar. Micropaleontol.*, 2:1-25.
- Kobayashi, K. (Ed.), 1989. *Preliminary Report of the Hakuho Maru Cruise KH-87-3, July-August 13, 1988, Izu-Ogasawara (Bonin), East Mariana Basin and Yap Trench (WESTPAC, ODP Site Survey)*: Tokyo (Ocean Research Institute, Univ. of Tokyo).
- McDuff, R. E., 1985. The chemistry of interstitial waters, Deep Sea Drilling Project Leg 86. In Heath, G. R., Burckle, L. H., et al., *Init. Repts. DSDP, 86*: Washington (U.S. Govt. Printing Office), 675-687.
- Ness, G., Levi, S., and Crouch, R., 1980. Marine magnetic anomaly time scales for the Cenozoic and Late Cretaceous. A précis, critique and synthesis. *Rev. Geophys. Space Phys.*, 18:753-770.

Ms 125A-111

NOTE: All core description forms ("barrel sheets") and core photographs have been printed on coated paper and bound as Section 4, near the back of the book, beginning on page 383.

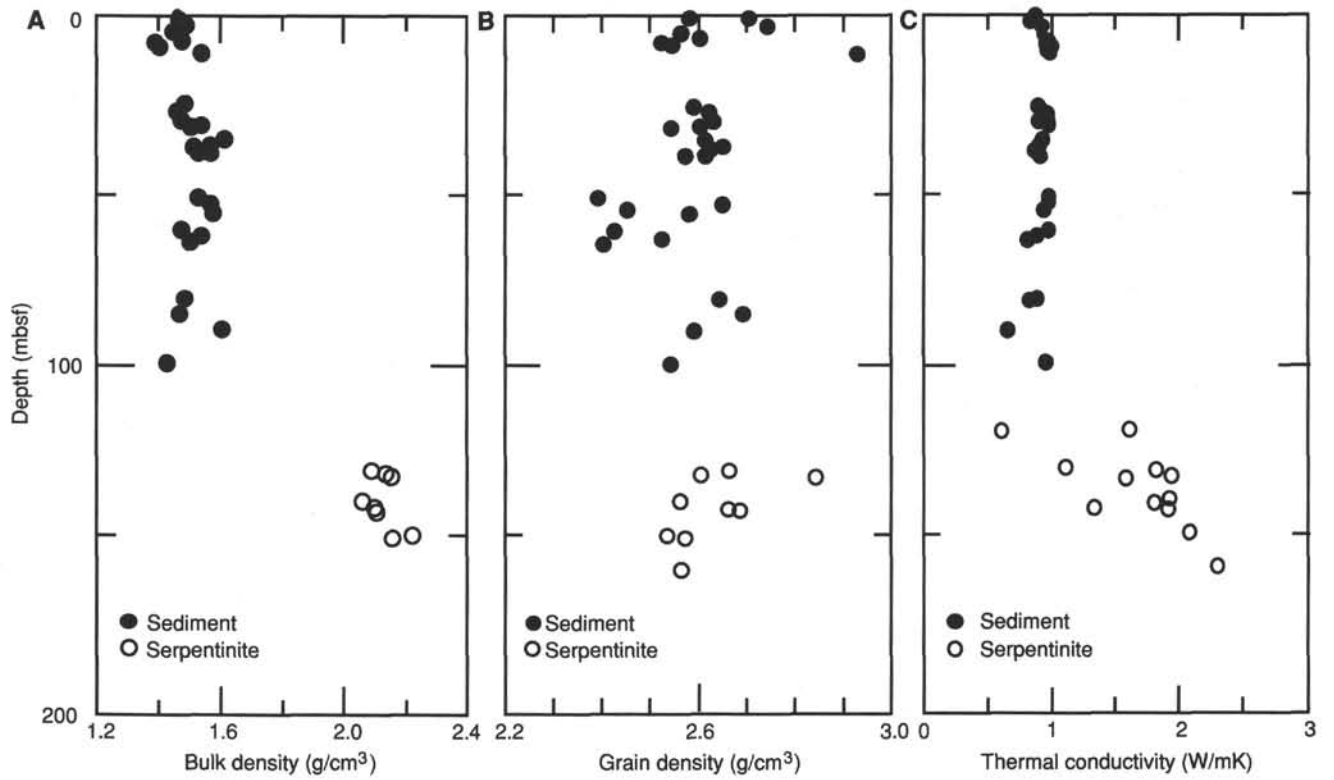


Figure 15. Physical and index properties vs. depth for Hole 783A. **A.** Bulk density (from discrete samples). **B.** Grain density. **C.** Thermal conductivity.

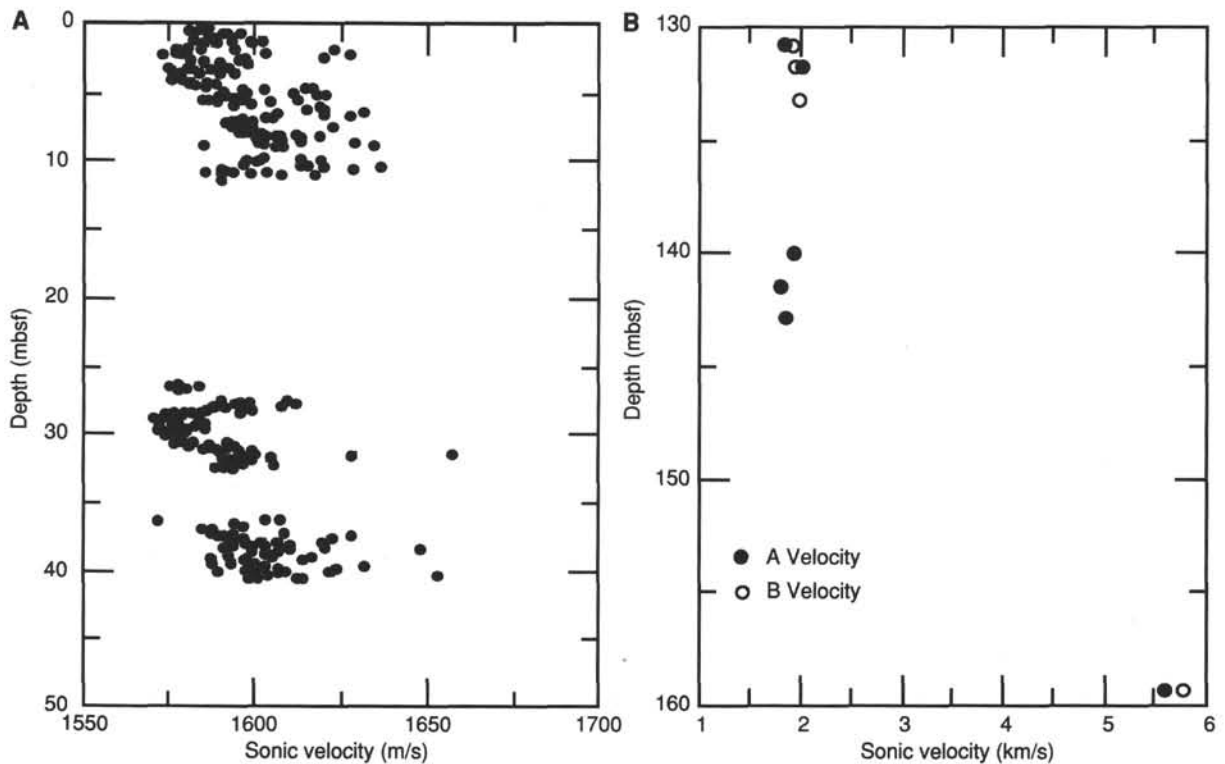


Figure 16. Sonic velocity vs. depth for Hole 783A. **A.** Velocity determined by the *P*-wave logger. **B.** Velocity determined from discrete samples; "A" velocities are parallel to core; "B" velocities are perpendicular to core.

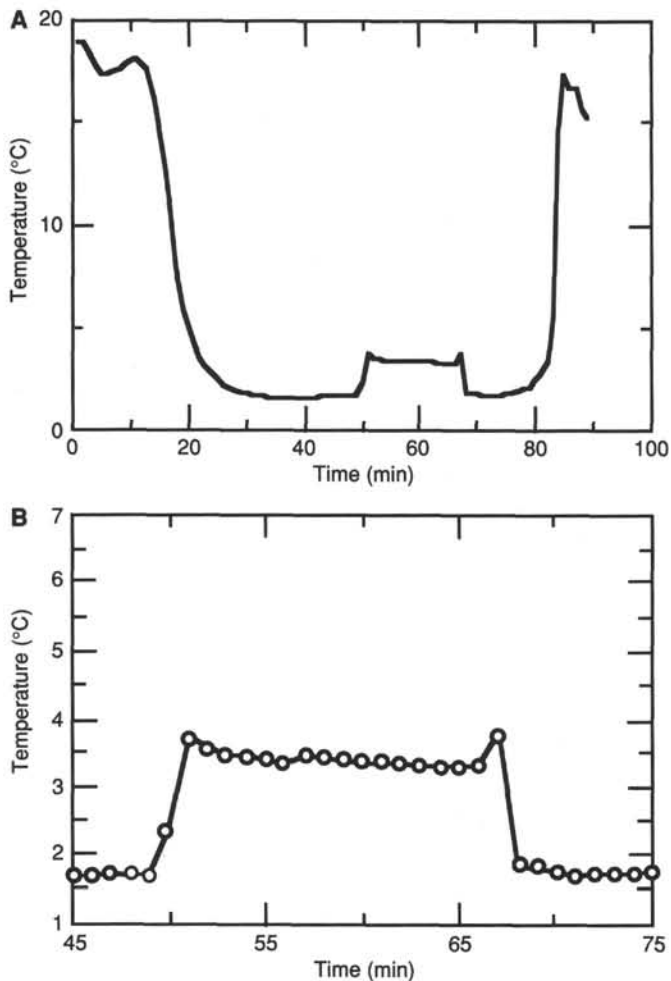


Figure 17. A. Temperature vs. time for Run 06R of the Barnes-Uyeda temperature tool at 42.7 mbsf in Hole 783A. B. An expanded plot showing the data when the tool was in the seafloor.

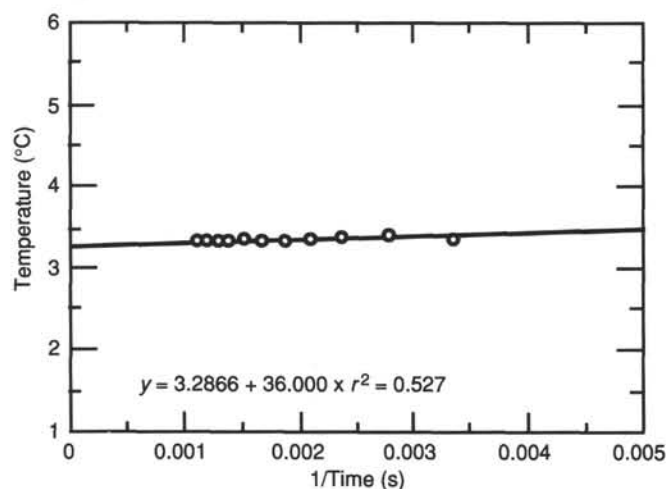


Figure 18. The reduced temperature fit of the first Barnes-Uyeda temperature run. The intercept value at 1/time = 0 is the equilibrium temperature of the sediment.

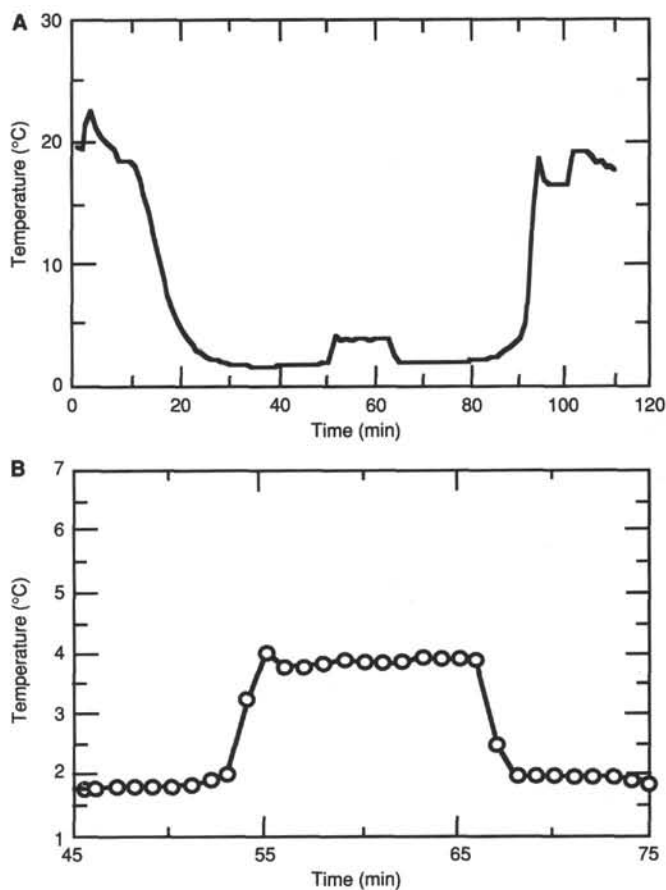


Figure 19. A. Temperature vs. time for Run 11R of the Barnes-Uyeda temperature tool at 90.9 mbsf in Hole 783A. B. An expanded plot showing the data when the tool was in the seafloor.

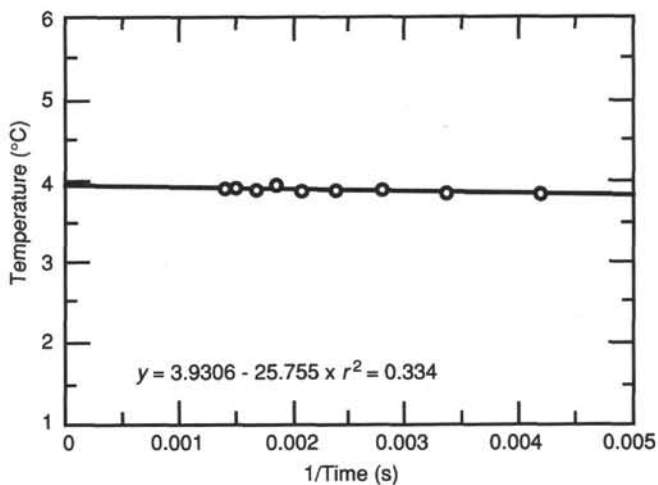


Figure 20. The corresponding reduced temperature fit for the second Barnes-Uyeda run.

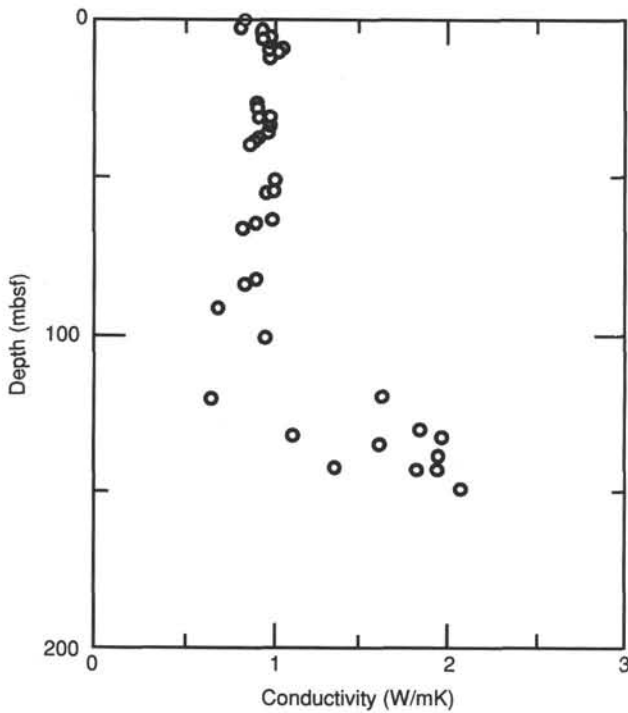


Figure 21. Plot of thermal-conductivity results vs. depth for Hole 783A.

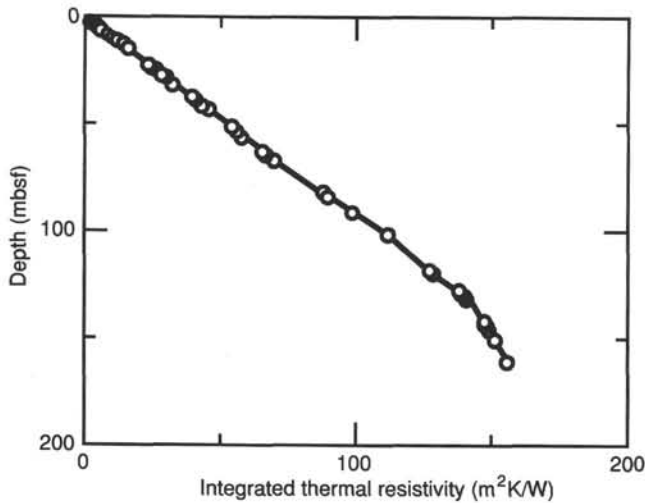


Figure 22. Plot of integrated thermal resistivity vs. depth for Hole 783A.

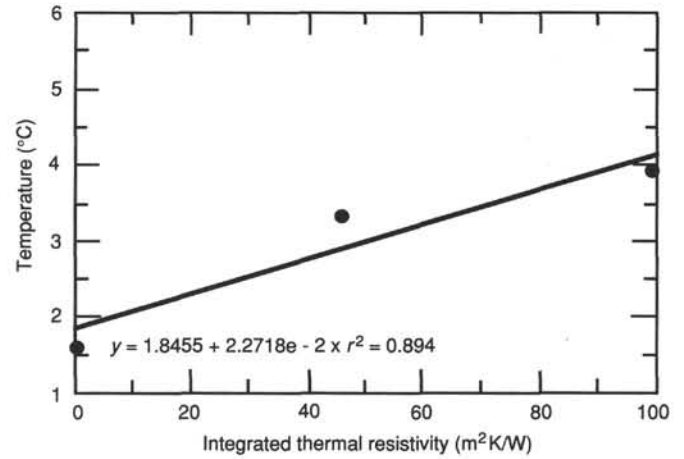


Figure 23. Temperature vs. integrated thermal resistivity for Hole 783A. The slope of the best-fitting linear regression is a heat-flow value of 23 mW/m². See text for discussion of possible explanations for the poor fit.

Age	Core	Recovery	Lith. unit	Lithology
middle or early Pleistocene	1R	■	I	Vitric clayey silt, glass-rich silty clay/claystone.
	2R	■		
	3R	■		
	4R	■		
	5R	■		
	6R	■		
	7R	■		
	8R	■		
	9R	■		
	10R	■		
early Pliocene	11R	■	II	Phacoidal, sheared serpentine with vertical convolute bedding.
	12R	■		
	13R	■		
	14R	■		
	15R	■		
	16R	■		
	17R	■		
	18R	■		

Figure 24. Core recovery and lithologic summary, Hole 783A.